Geophys. J. Int. (2003) **155,** 93–110

Coseismic and early post-seismic slip associated with the 1999 Izmit earthquake (Turkey), from SAR interferometry and tectonic field observations

Ziyadin Çakir,[1,*] Jean-Bernard de Chabalier,[2] Rolando Armijo,[2] Bertrand Meyer,[2] Aykut Barka[1] and Gilles Peltzer[3]

[1] *ITU, Istanbul, Turkey. E-mail: cakirz@itu.edu.tr*
[2] *IPGP, CNRS, UMR* 7578 *and* 7580, *Paris, France*
[3] *JPL, Caltech,* CA 91109, *USA*

Accepted 2003 March 31. Received 2003 February 18; in original form 2002 July 16

SUMMARY

We use combined tectonic field observations and SAR data to determine an improved model of the slip associated with the 1999 Izmit earthquake, which ruptured the North Anatolian Fault at the eastern end of the Sea of Marmara. The leading goal is to understand the main features of the coseismic and post-seismic deformation, which are captured together in the SAR data. To achieve this, we make a critical analysis of the ERS1-2 SAR data, which allows atmospheric effects to be identified and removed. We also use detailed field mapping and measurements of the earthquake surface rupture. Dislocations in elastic half-space and a forward modelling strategy allow us to obtain a slip model by steps. A trial-and-error approach is combined with conventional inversion techniques to determine the slip in the different regions of the fault. The SAR data are well explained with three main zones of high slip along the fault, releasing a total moment of 2.3×10^{20} N m ($M_w = 7.6$), which is higher than the seismological estimates ($1.7–2.0 \times 10^{20}$ N m). The inhomogeneous slip distribution correlates with fault segments identified at the surface. The Izmit rupture appears to have extended 30 km west of the Hersek peninsula into the Sea of Marmara with slip tapering from 2 m to zero. The western end of the rupture is located 40 km SSE from Istanbul. We show that some features seen near to Mudurnu and Gevye and previously interpreted as slip on secondary faults are explained mostly as atmospheric effects correlated with the topography. Using our approach and the available GPS data we obtain a slip model that represents the coseismic slip alone, which suggests that the moment release during the main shock was 1.9×10^{20} N m ($M_w = 7.5$), consistent with the seismological estimates. We conclude that the SAR data include the effects of 2 m of fast after-slip during the month following the main shock, within a zone of the fault located 12–24 km below the epicentral region. Near the hypocentre at a depth of 18 km, the fault appears to have experienced dynamic slip of 1 m associated with the main shock, followed by 2 m of rapidly decelerating post-seismic shear during the following month. We suggest that the distribution of heterogeneous slip and loading along the different fault segments may be important factors controlling the propagation of large earthquake ruptures along the North Anatolian Fault.

Key words: Izmit earthquake slip, coseismic, post-seismic deformation, InSAR.

INTRODUCTION

The potential for the occurrence of moderate and large earthquakes along large strike-slip faults such as the North Anatolian or the San Andreas faults depends on the length to which a seismic rupture can propagate. In turn, the rupture length depends on many factors, such as the degree of geometric complexity of the fault surface, its roughness, the local state of tectonic loading preceding the event and the rupture dynamics during the event. Besides, slip during an earthquake is known to distribute heterogeneously along the fault, a feature that can be attributed to variation in frictional slip processes (Tse & Rice 1986). In this paper we address the distribution of slip that occurred during and soon after the Izmit earthquake in Turkey, using tectonic field observations and geodetic SAR data that cover

*Now at: Institut de Physique du Globe, Strasbourg, France. E-mail: ziyadin.cakir@eost.u-strasbg.fr.

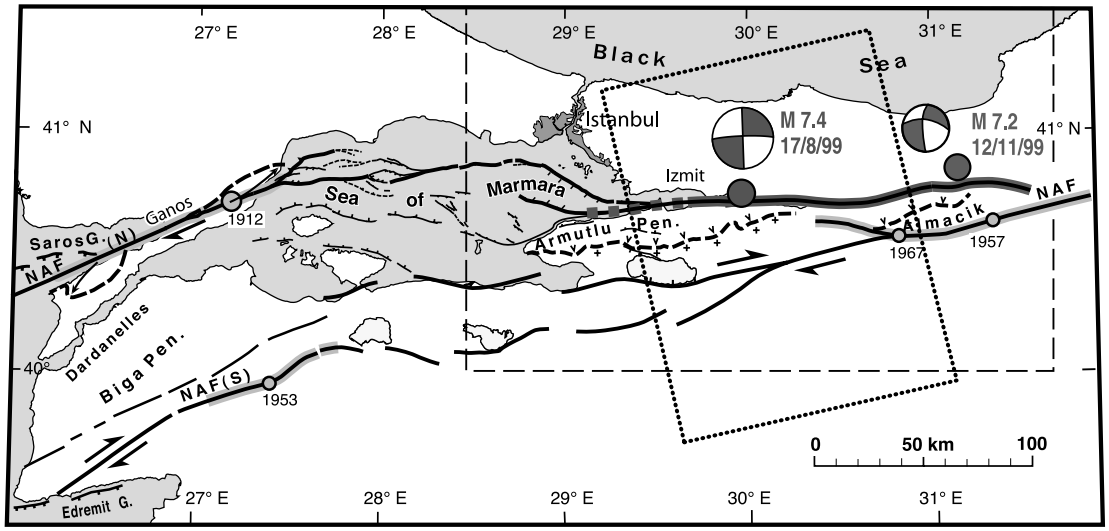

Figure 1. Active faulting in the Marmara pull-apart region (from Armijo *et al.* 1999, 2002). The North Anatolian Fault (NAF) splays westwards into a northern (N) branch and a southern (S) branch 100 km apart. Faults associated with recent earthquake breaks are outlined in light and dark grey. The 1999 events occurred along a prominent fault splay east of Marmara. Fault-plane solutions from the USGS catalogue. The dashed and dotted rectangles outline, respectively, the area enlarged in Fig. 2 and the location of interferograms in Fig. 3.

the event as well as 1 month of post-seismic deformation. Our aim is to characterize the different domains where unstable (coseismic) and stable (aseismic) slip may have occurred along different segments along strike and particularly in the transitional zone at 12–18 km depth, where the earthquake nucleated.

The 1999 August 17 Izmit earthquake ($M_w = 7.4$ from long-period waves) ruptured a portion of the plate boundary between Anatolia and Eurasia along the North Anatolian Fault (NAF) (Fig. 1). The event was preceded by a sequence of six large earthquakes that ruptured the NAF progressively from east to west during the 20th century (Barka & Kadinsky-Cade 1988; Barka 1996; Stein *et al.* 1997; Nalbant *et al.* 1998). The Izmit event was also followed, 3 months later on 1999 November 12, by another destructive earthquake ($M_w = 7.2$) that ruptured the neighbouring Düzce Fault, east of the Izmit Fault (Akyüz *et al.* 2002). Within the next few decades large similar earthquakes are expected to rupture the submarine fault system that extends west of the Izmit Fault under the Sea of Marmara, adjacent to the city of Istanbul (Barka 1999; Hubert-Ferrari *et al.* 2000; Parsons *et al.* 2000; Atakan *et al.* 2002).

Soon after the event, the Izmit Fault rupture was mapped in the field by an international team (Barka *et al.* 2002; Hartleb *et al.* 2002; Langridge *et al.* 2002; Rockwell *et al.* 2002). This allowed the surface fault geometry to be determined and the variation of slip along strike to be measured with accuracy, due to the presence of numerous markers of human origin which were offset across the fault (roads, railways, canals, walls, fences). However, the exact length of the rupture remained undetermined, because some tens of kilometres of its western extension under the eastern Sea of Marmara could not be observed directly.

Several studies using various data sets (near-field strong motion records, far-field body waves, GPS measurements and SAR interferometry) have attempted to characterize the coseismic slip distribution, leading, however, to significantly differing results (Bouchon *et al.* 2000; Reilinger *et al.* 2000; Yagi & Kikuchi 2000; Tibi *et al.* 2001; Wright *et al.* 2001; Bürgmann *et al.* 2002; Delouis *et al.* 2002; Feigl *et al.* 2002). The SAR interferograms obtained with ERS data of the Izmit earthquake contain some signal due to a heterogeneous troposphere. These effects were encountered in previous studies and so the SAR data were considered less reliable than other independent data sets (e.g. Reilinger *et al.* 2000; Delouis *et al.* 2002). Using two tandem ERS1–ERS2 pairs, the topography and the meteorological data, some of the atmospheric effects can be identified with confidence and removed.

Together the corrected SAR data and the tectonic observations provide an accurate and complete description of the surface deformation associated with the Izmit earthquake. Combining the two data sets allows us to determine the slip distribution with depth for the different segments that ruptured. We proceed using a trial-and-error approach to explore solutions consistent with the tectonic information, then an inversion technique to improve the fit to the SAR data. Our approach explains the discrepancies between models deduced earlier from other data sets. Our final solution is a slip distribution that represents the coseismic slip and 1 month of post-seismic deformation captured by the SAR data. We use the data from temporary and permanent GPS stations to separate the coseismic from the post-seismic slip, and thus to estimate the amount, rate and depth distribution of the aseismic slip relative to the coseismic slip. Finally, we discuss the implications of slip heterogeneity, aseismic slip and fault segmentation in relation to the short-period seismological results and the long-term geological evidence.

TECTONIC BACKGROUND, FIELD OBSERVATIONS OF THE SURFACE BREAK, DISTRIBUTION OF AFTERSHOCKS AND BATHYMETRY OF THE EASTERN SEA OF MARMARA

Unlike the previous earthquakes of the 20th century sequence, which broke 700 km along the linear eastern and central parts of the NAF, the 1999 Izmit and Düzce events ruptured a fault splay at the entrance of the more complex Sea of Marmara pull-apart region (Fig. 1). In this region the NAF divides into a number of fault branches involving significant subsidence and crustal extension (Barka & Kadinsky-Cade 1988; Parke *et al.* 1999; Armijo *et al.* 1999, 2002). The 1999 earthquakes occurred close to where two previous events had already

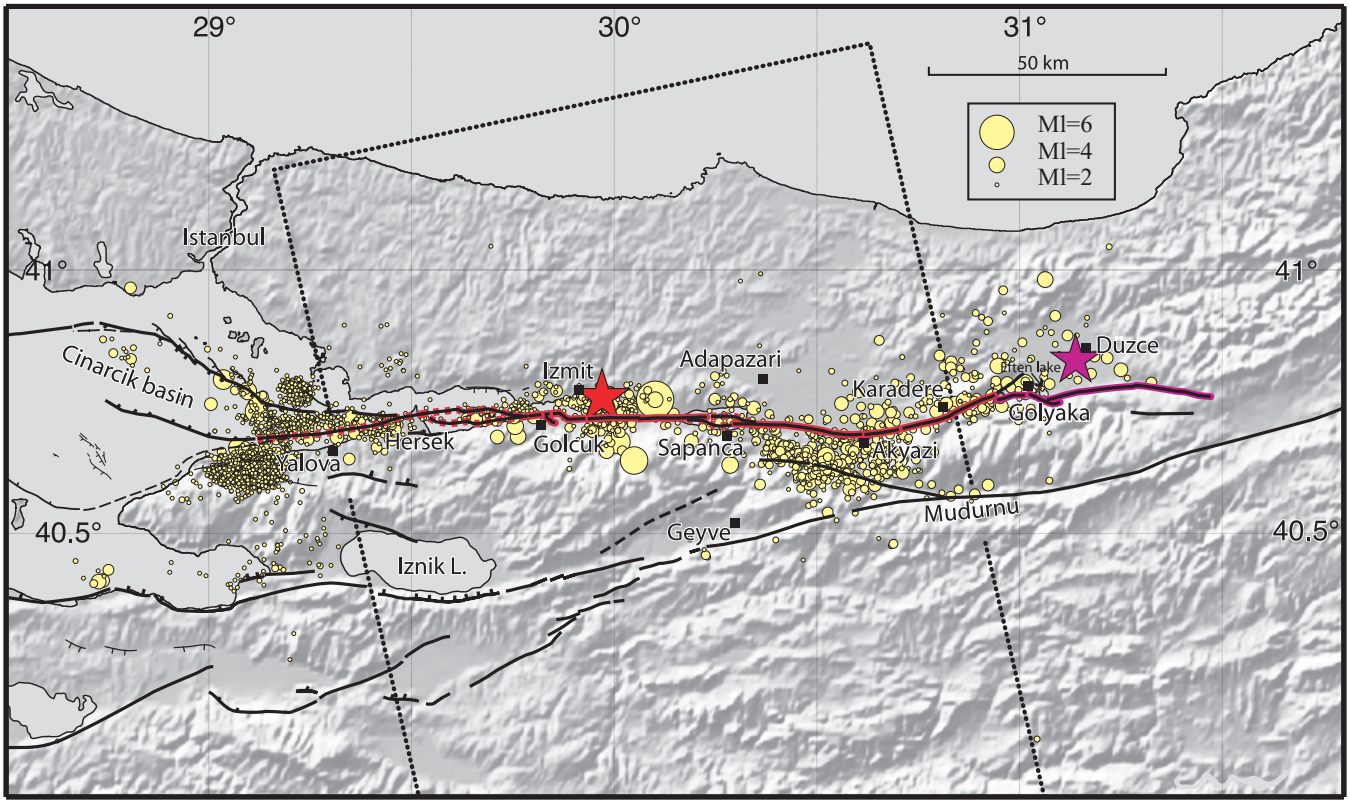

Figure 2. Fault segments and the breaks of the 1999 earthquake. Breaks of the Izmit (1999 August 17) and Düzce (1999 November 12) events are highlighted in red and purple, respectively. Stars denote epicentres of main shocks. Yellow circles are $M_L \geq 2$ aftershocks recorded between 1999 August 20 and October 20 by the Tübitak permanent network (Özalaybey *et al.* 2002) and by a temporary array (Karabulut *et al.* 2002). The background DEM image is from GTOPO 30. The Izmit break has 110 km length on land but secondary features and aftershock distribution suggest that it extends 50 km west of Gölcük, beyond the Hersek peninsula and offshore Yalova (dashed red lines).

ruptured in 1957 and 1967 contiguous fault segments south of the Almacik block (Fig. 1). Together the Izmit and Düzce earthquakes ruptured almost completely the sinuous fault branch north of the Almacik block, so this block is now surrounded by the recent breaks. A prominent fault bend characterizes the surface rupture near the city of Akyazi (Fig. 2). It may be explained by the long-term counter-clockwise rotation of the Almacik block with respect to Eurasia (Armijo *et al.* 1999, 2000). The geological evidence also indicates that the earthquakes ruptured the main branch of the NAF entering the Sea of Marmara at the Gulf of Izmit. This branch becomes gradually more extensional westward, as larger and larger fault step-overs and deeper pull-apart basins filled with sediment occur along it (e.g. Barka & Kadinsky-Cade 1988; Armijo *et al.* 2002, see Fig. 2).

Detailed observations and maps of the Izmit earthquake surface rupture are reported by Barka *et al.* (2002). Here we summarize the main results relevant to this study. The rupture was observed on land over a total length of 110 km. It is composed of a series of segments with overall E–W strike and mainly right-lateral slip. Seen in more detail, the strike of the rupture changes gradually to N80°E as it enters the Sea of Marmara and bends to a N70°E strike as it reaches the Almacik block.

Four main strike-slip segments are distinguished along the Izmit rupture, from west to east (Fig. 2): the Gölçük, the Izmit–Sapanca, the Sapanca–Akyazi and the Karadere segments. Two clear extensional step-overs separate the first three segments, at the Izmit Bay immediately east of Gölçük and at the Sapanca Lake. The Karadere segment forming the eastern end of the rupture has an ENE strike and its connection with the main rupture at the Akyazi fault bend is unclear. Another step-over is at the very eastern end of the rupture near Gölyaka and the Eften Lake. This area experienced up to 20 cm of right-lateral slip during the Izmit (August) event and much more (>5 m) lateral and normal slip during the subsequent Düzce (November) event (Akyüz *et al.* 2002; Hartleb *et al.* 2002).

Coseismic slip could be measured with precision along the fault trace. Significant slip variability was observed at the scale of the superficial complexities along the break (multiple mole-track branches and small stepovers), within a generally narrow fault zone (1–50 m). Consequently, measurements of small markers sample fractions of the total deformation and usually underestimate the actual slip across the fault zone. The slip appears less variable whenever large man-made markers crossing the fault (such as roads, railways and canals for irrigation) could be surveyed. Such surveys integrate the deformation across the fault zone better and are thus more reliable than the local measurements of smaller markers, to which they provide upper bounds. Fig. 5(b) (see later) incorporates our best estimates of coseismic slip obtained from these surveys.

Maximum right-lateral slip exceeding 5.5 m was measured in two areas, east of the Sapanca Lake and in the city of Gölçük. Vertical slip was generally minor, but locally it reached 2.3 m over the oblique NW-striking normal faults that bound the Izmit Bay extensional step-over east of Gölçük. The hypocentre where the earthquake appears to have nucleated is to the east of the Izmit Bay and 5–10 km east of the region of maximum slip in Gölçük (Figs 2 and 5).

Table 1. ERS data and interferograms used in this study (track 157 frame 815). Ha is the altitude of ambiguity (the magnitude of unmodelled topography required to create one fringe).

First orbit No, date	Second orbit No, date	H_a (m)	Interval (days)	Interferogram
42229, 1999 August 12	42730, 1999 September 16	3147	35	ERS1
22556, 1999 August 13	23057, 1999 September 17	329	35	ERS2
42229, 1999 August 12	23057, 1999 September 17	42	36	ERS1–ERS2
22556, 1999 August 13	42730, 1999 September 16	38	34	ERS2–ERS1
42229, 1999 August 12	22556, 1999 August 13	41	1	August tandem
42730, 1999 September 16	23057, 1999 September 17	40	1	September tandem

West of Gölçük (Fig. 2) the rupture continued to an unknown extent under water, possibly along the edges of, and/or across, the elongated pull-apart feature seen in the bathymetry between Gölçük and the Hersek peninsula (Kuscu *et al.* 2002). The Gölçük strike-slip segment must be short (less than about 5 km), because it is immediately flanked both to the east and the west by significant step-overs with normal and oblique slip. Many large slumps that occurred all along the coastal area between Gölçük and Hersek were interpreted as lateral spreading effects of the submarine part of the earthquake rupture. However, no evident surface break was observed across the Hersek peninsula. Only some minor cracks were noticed in the ground near the tip of the peninsula, where the long-term morphology indicates the passage of a large strike-slip fault. This has led to the inference that the surface break of the Izmit earthquake ended somewhere east of the Hersek peninsula, with a total rupture length limited to 130 km.

The distribution of well-located aftershocks suggests a longer rupture, possibly including the Yalova–Hersek segment, west of Hersek (Ito *et al.* 2002; Karabulut *et al.* 2002; Özalaybey *et al.* 2002) (Fig. 2). Apart from aftershocks outlining the overall surface rupture, three regions hosted significant swarms; south of Akyazi, around the epicentre at Izmit, and north and west of Yalova. In fact, three swarms of aftershocks are located definitely west of the Hersek peninsula (Karabulut *et al.* 2002).

High-resolution bathymetric data acquired recently indicate that west of the Hersek peninsula and north of Yalova the submarine fault system splays apart into two main branches that veer towards a NW strike, as the depth to the sea bottom increases dramatically (Fig. 2) (e.g. Armijo *et al.* 2002). These two fault branches have a significant long-term antithetic normal component of slip. They run at the base of the two large escarpments that bound the 1150 m deep Cinarcik Basin, which appears to be one of the largest pull-apart basins in the Sea of Marmara (Barka & Kadinsky-Cade 1988; Armijo *et al.* 2002). In a later section we use the bathymetry, aftershock locations and the SAR interferometry to determine the probable extent, the geometry and the slip distribution of the Izmit rupture in this submarine region.

THE INSAR DATA AND THE ATMOSPHERIC EFFECTS

We calculated several interferograms that span the 1999 Izmit earthquake both in the descending and ascending modes of the European Space Agency's ERS1 and ERS2 satellites. Of these, only two ascending interferometric pairs have high coherence and give a good image of surface deformation associated with the earthquake. The two interferograms are formed by combining two pairs of tandem images of ERS1 and ERS2 acquired several days before the event in August (orbits ERS1-42229, ERS2-22556, 12–13 August) and about a month after (orbits ERS1-42730, ERS2-23057, 16–17 September) (Table 1, Fig. 3).

We used the two-pass method (Gabriel *et al.* 1989; Massonnet *et al.* 1993) in which the topographic contribution to the interferogram is removed using a digital elevation model (DEM). The ERS2

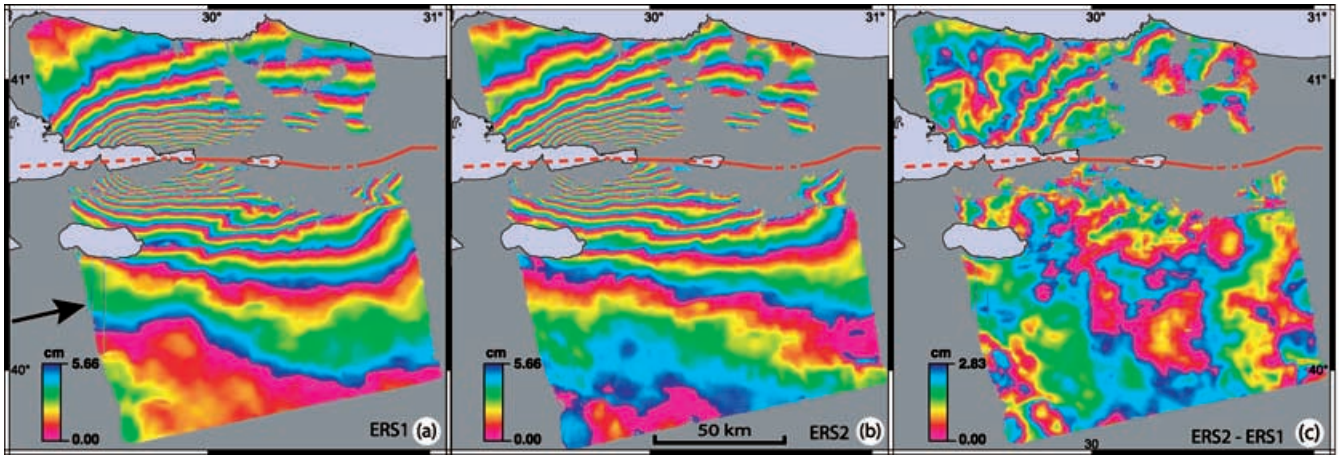

Figure 3. Interferograms of the Izmit earthquake. Data are from ESA satellites ERS1 and ERS2 acquired during ascending orbits. Surface rupture of Izmit earthquake is outlined in red. Each fringe (one full colour cycle) represents 5.6 cm of range change along the radar line of sight (see text) whose horizontal projection is indicated by a black arrow. Positive changes indicate that distance to satellite has increased. (a) ERS1 interferogram (12 August–16 September 1999). (b) ERS2 interferogram (13 August–17 September 1999). (c) Phase difference between the ERS1 and ERS2 interferograms. Here one fringe corresponds to a range change of 2.8 cm. The four to five fringes seen in the north-eastern part of the interferogram are not correlated with topography and are likely to be the consequence of a heterogeneous troposphere.

interferogram is constructed using precise orbits calculated by the University of Delft (Scharroo & Visser 1998) and thus we assume it does not contain orbital residuals significant enough to be removed (more than one fringe across the image). However, the precise orbits were not available for the ERS1 interferogram and therefore it may contain orbital fringes. This problem can be solved by removing the difference between the two interferograms attributable to orbital precision, in this case a plane that contains two and a half fringes running roughly parallel to the satellite direction of flight. For the relatively simple Izmit rupture this correction is enough to resolve tectonic deformation in the far field, so orbital parameters are not included in our inversion procedure.

The interferograms are filtered using a weighted power spectrum algorithm (Goldstein & Werner 1998) and then coherent fringes (about 87 per cent) are automatically unwrapped and sampled to be used for modelling. To have a clear view of the surface deformation (shape, gradient and the number of fringes), we present the interferograms in Fig. 3 rewrapped with fringes, each fringe representing a range change of 5.66 cm (one wavelength) along the radar line of sight. Because the interferograms span a time interval ending about 1 month after the event, they must contain some centimetres of range change due to post-seismic deformation as deduced from the GPS measurements (Reilinger *et al.* 2000; Bürgmann *et al.* 2002; Ergintav *et al.* 2002; Feigl *et al.* 2002; Hearn *et al.* 2002).

Despite the rough topography and dense vegetation cover, the coherence is fairly good over large parts of the interferograms. It is lost in areas close to the fault (blank areas within the image frame). This may be partly due to the steep slip gradient in these areas. However, clear fringes can be observed within a few kilometres from the surface rupture along the southern side of the Izmit–Sapanca segment. Decorrelation also occurs in the flat areas in the central and western parts of the interferograms, which is probably due to changes in the water content in the soils.

Because the displacement associated with the right-lateral strike slip occurs mostly in the E–W direction, that is nearly parallel to the radar line of sight, the fringes are mostly symmetric about the fault trace. The symmetry of fringes running parallel to the fault also suggests that the fault is very steep. However, in the central part of the interferograms the fringe rate appears higher on the northern side of the fault than on its southern side. This feature may indicate that the fault dips steeply to the north, in agreement with the focal mechanism of the main shock (Harvard CMT). The area of Izmit and Gölçük appears surrounded by elliptical-shaped fringes with high rate, consistent with the large amounts of slip observed there. Fringes with high rate are seen east of Gölçük towards the Hersek peninsula, and more spaced fringes continue for at least 15 km westwards beyond Hersek. Several fringes appear deflected in two particular places: along the Mudurnu valley southeast of Akyazi and along the northwestern edge of the Geyve Basin, south of Sapanca. These features appear to be along known faults but also appear to correlate with sharp topographic features. The possibility that these features result from motion on secondary faults dynamically triggered by motion on the main fault has been explored (Armijo *et al.* 2000; Wright *et al.* 2001; Feigl *et al.* 2002). We re-examine this possibility and explore further the hypothesis of atmospheric effects correlated with the topography.

The main difference between the two interferograms is on the northern side of the fault. There the fringes in the ERS2 interferogram trend more NE on the western side and more NW on the eastern side, making a broad concave-southwards cusp. Subtracting one interferogram from the other shows that the ERS2 data contain at least two more fringes—or a maximum of 14 cm range change—in this cusp region (Fig. 3c). This difference requires explanation before modelling the earthquake faulting process. There appears to be no correlation between the fringes in Fig. 3(c) and topography, in contrast with examples of similar features studied elsewhere (Delacourt *et al.* 1998; Beauducel *et al.* 2000). Therefore, these fringes are very likely to be a consequence of a heterogeneous troposphere (Feigl *et al.* 2002). It is not possible, however, to use a perfect 'pairwise logic' (Massonnet & Feigl 1998) to determine whether one of the radar images contains most of the atmospheric effect. This is because the orbital separation combining ERS1–ERS2 pairs are not suitable for obtaining coherent interferograms (see Table 1). Here we use a comparable strategy, which is developed below.

The two 1-day ERS1–ERS2 tandem pairs can be processed. With such a short time period both tandem interferograms should be very coherent and contain practically no surface deformation. However, coherence is almost completely lost in the southern and northwestern regions in both interferograms, which is probably due to small altitudes of ambiguity (Table 1). The signal is poorly structured and almost negligible in the August tandem interferogram (Fig. 4a). In contrast the September tandem interferogram contains in its coherent part an organized signal of up to three fringes (Fig. 4b). These fringes have an elliptical shape over a wide region that is the same as that of the cusp seen in the difference between the two coseismic interferograms (Fig. 3c). The features seen in the September tandem pair are thus very likely to correspond to local atmospheric effects of meteorological origin, at the scale of the interferogram, much like similar features described elsewhere (cf. Massonnet & Feigl 1998).

We have checked the available meteorological data to see whether atmospheric changes occurred during the time interval when the SAR tandem data were acquired, during 1999 September. Two of the NOAA satellite images acquired on the days of ERS data acquisitions are shown in Figs 4(c) and (d). The sky is clear in the Sea of Marmara region about 13 h before the ERS1 data acquisition (16 September) (Fig. 4c). However, clouds cover the area to the north and to the northeast of the Gulf of Izmit approximately 7 h before the acquisition of the ERS2 data (17 September) (Fig. 4d). This change suggests that the atmospheric and weather conditions were rapidly degrading from September 16 to 17. Accordingly, the atmospheric effects seen in the September tandem interferogram are most probably included in the ERS2 image, which explains why the ERS2 coseismic interferogram has more fringes than the ERS1 one. In addition, the good atmospheric conditions prevailing on the 16th September are similar to those seen in the NOAA data covering 1999 August 12 and 13 (that we do not show), when the first tandem pair was acquired.

Therefore, we prefer not to use the ERS2 interferogram to deduce the source parameters of the Izmit event, in contrast with earlier published work (Delouis *et al.* 2002; Wright *et al.* 2001).

MODELLING THE SLIP DISTRIBUTION

The purpose of our modelling procedure is to determine a set of source parameters explaining both the tectonic observations and the SAR data. As in other examples elsewhere in the world, the SAR data set appears to be the best for deducing an overall image of the static rupture at seismogenic depth. Although with similar accuracy (within an error of less than 1 cm), the GPS measurements sample discrete observation points with generally no comparable spatial coverage. However, GPS measurements provide true displacement vectors. For the Izmit event the GPS data have been used to model slip (Reilinger *et al.* 2000; Bürgmann *et al.* 2002; Feigl *et al.* 2002)

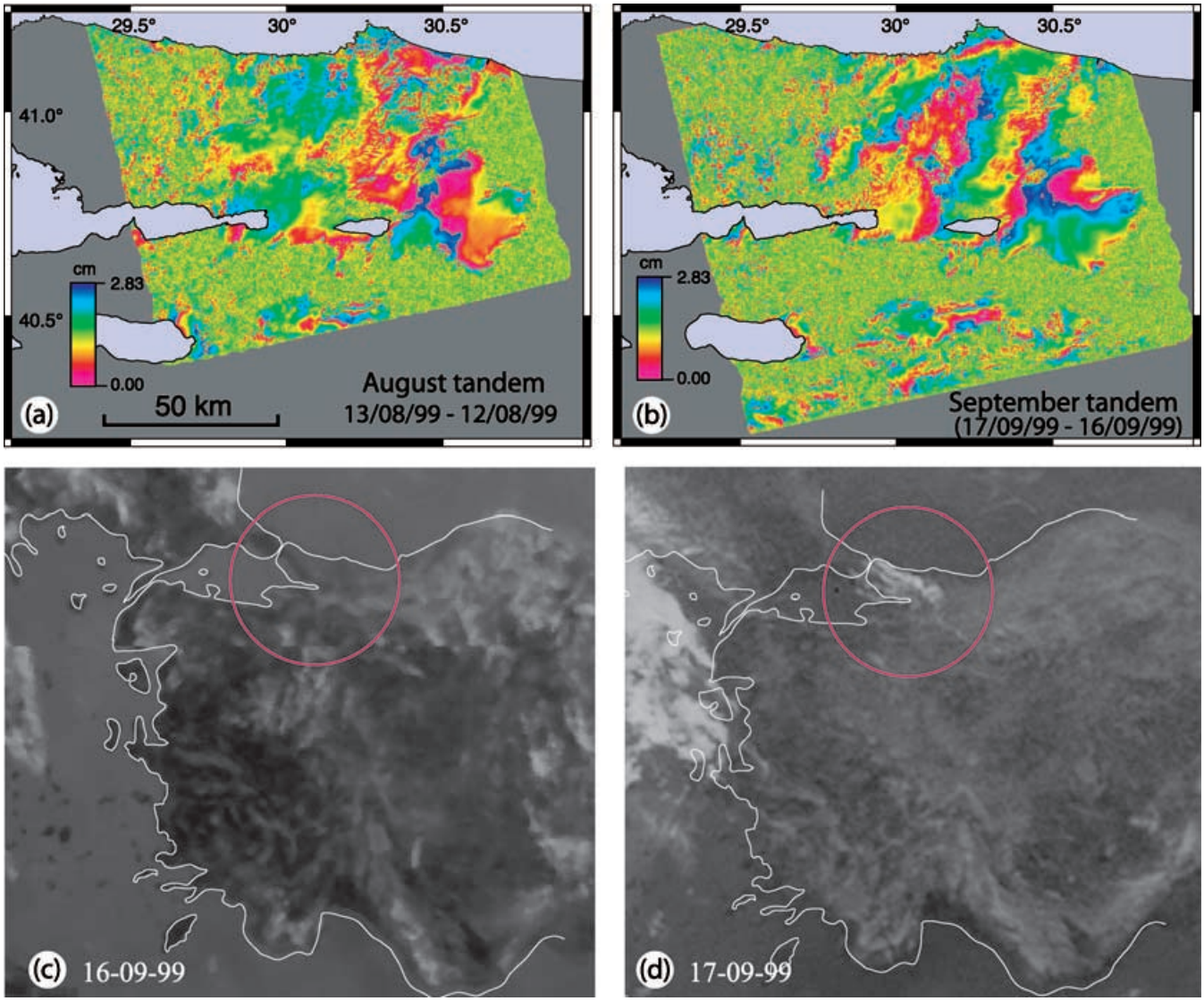

Figure 4. Identification of atmospheric effects. Tandem interferograms calculated from ERS1 and ERS2 images: (a) 12–13 August 1999 interferogram. (b) 16–17 September 1999 interferogram. Each fringe represents 2.8 cm of ground shift away from satellite along the radar line of sight. The fringes seen in the northern part of the September interferogram confirm the occurrence of tropospheric effects. (c, d) Meteorological data; NOAA DMSP images acquired on 16 (c) and 17 (d) September 1999. The circle locates the study area. The tropospheric effects encountered in the ERS2 interferogram appear related to the presence of clouds just before the acquisition of the 17 September ERS2 data.

and in a later section we discuss the main implications of this data set in view of our own results.

The quality of the SAR data is generally poor close to the rupture trace, due to lack of coherence. Pixel offsets across the fault trace in the SAR amplitude images can be used to determine the surface slip (Michel *et al.* 1999; Peltzer *et al.* 1999). However, for the Izmit earthquake the results obtained with this technique are too scattered and thus of little use. A similar technique using SPOT satellite images provided good results only along one of the segments of the Izmit rupture (the Izmit–Sapanca segment; Michel & Avouac 2002). The particularly precise measurements of offset markers gathered in the field after the event provide an overall coverage of the surface rupture (Fig. 5b) and the slip observed is consistent with the SPOT data where the latter are available.

To model the ERS1 interferogram we use dislocations on rectangular planes embedded in an elastic half-space (Okada 1985). We use a forward modelling strategy to obtain a first-order model that is then refined by steps combining a trial-and-error approach with a conventional inversion technique. The procedure seeks to fit the SAR data that are sampled uniformly where the interferogram is coherent, in this case 14 000 samples of range change measured in the ERS1 interferogram. The shift between regions of the interferogram to the north and south of the fault is fixed by fitting models to the far field and checking for consistency with the GPS vectors (Reilinger *et al.* 2000; Bürgmann *et al.* 2002).

Our first-order model (model I) is obtained with a simplified fault divided into vertical patches 5 km long along strike, consistent with the geometry of the observed surface rupture on land and with the features seen in the bathymetry of the Sea of Marmara. Slip is purely right-lateral strike-slip, consistent with the measurements gathered at the surface for each patch and extrapolated uniformly down to 18 km depth (Fig. 5, I). This is the overall depth for which forward modelling gives the best fit to the SAR data (rms of 2.4 cm in range). The resulting geodetic moment is 2.5×10^{20} N m, which is

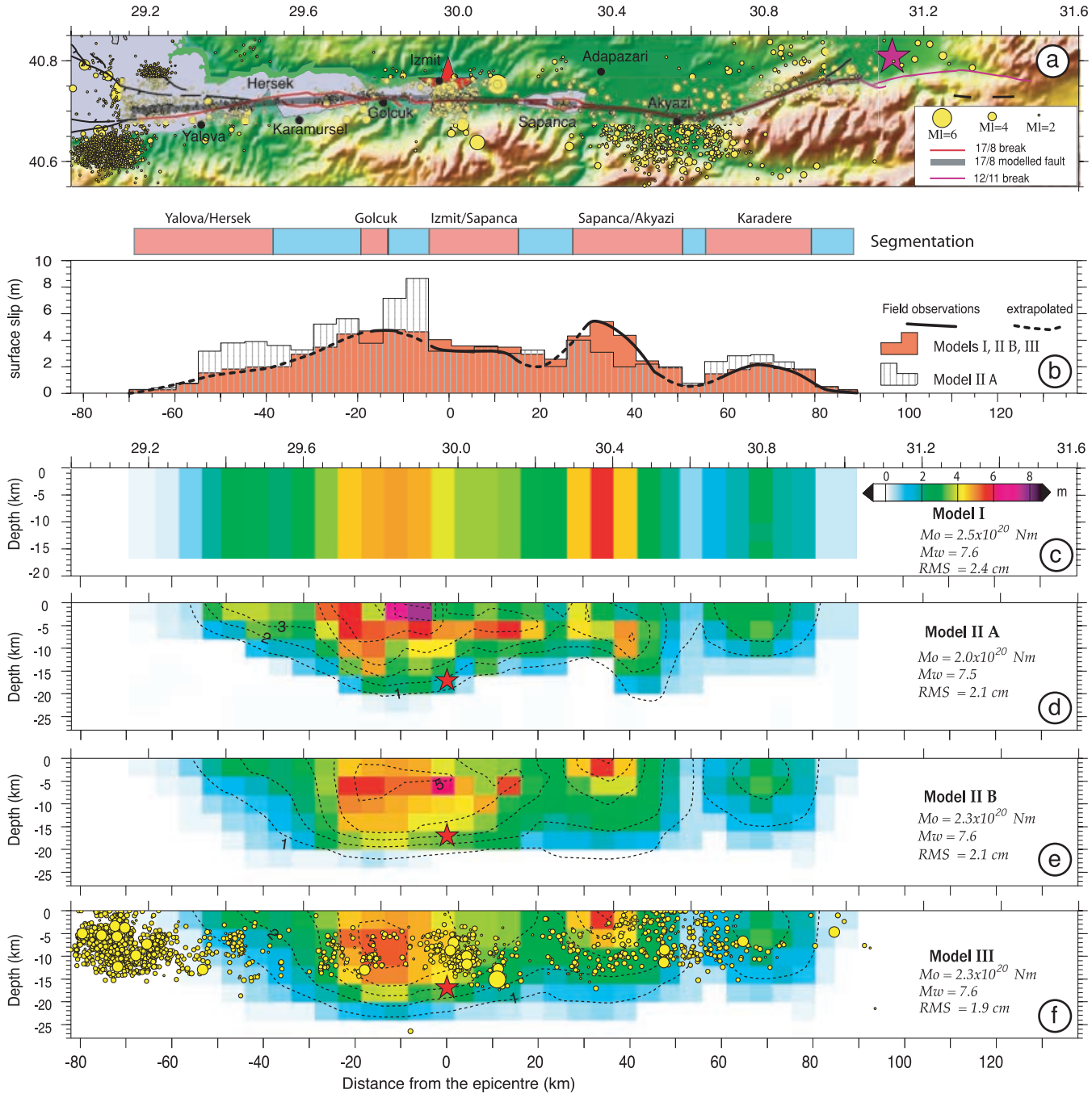

Figure 5. The Izmit earthquake fault trace, the coseismic surface slip and the modelled slip distribution at depth. (a) Shaded topographic map with fault segments and simplified fault trace. Surface breaks (thick line) of the Izmit (red) and Duzce (purple) events are indicated. Locations of mainshocks (stars) and of aftershocks (yellow circles) as in Fig. 2. (b) Surface right-lateral slip projected along the fault trace. The sinuous curve in bold integrates the most robust field measurements (dashed where extrapolated). The toothed graph in orange represents the discrete values used for modelling slip at depth in 32 fault patches with 5 km length along the fault strike (model I). The hatched graph is the surface slip obtained by inversion in IIA. Segments and intersegment regions are indicated on top, by pink and light blue stripes, respectively. (c) Model I: first-order forward modelling of slip distribution. Slip is purely right-lateral (in m). Slip variation along strike is consistent with the tectonic observations and is extrapolated in vertical fault patches to variable depth to fit the SAR data. Best fit is for uniform fault depth of 18 km. Red star represents main shock hypocentre. (d) Model IIA: obtained by inversion of slip in a fault with 224 vertical patches $5 \times 4\ \mathrm{km}^2$. Slip is inverted using model I as initial slip distribution. Lines of equal slip are in metres. Resulting slip in the patches near the surface (0–4 km depth) is represented in b (hatched graph). (e) Model IIB: Inversion model with slip fixed for the patches near the surface (0–4 km depth). (f) Model III: Obtained by inversion of slip in a fault slightly dipping north, using initial slip close to model IIB. Izmit–Sapanca and Sapanca–Akyazi segments have uniform 85° dip to the north and 176° rake, other segments are vertical. Mainshock (red star) and aftershocks (yellow circles) projected along fault strike. Scalar moment (M_o) magnitude (M_w) and rms to the ERS1 data are indicated for each model.

equivalent to a moment magnitude of $M_w = 7.6$. The implied fault rupture is about 160 km long from Gölyaka to approximately 30 km west of the Hersek peninsula. Below we discuss more precisely how the western end of the rupture is constrained by the SAR data. Overall, our first-order model is similar to that discussed for the ERS2 interferogram in Armijo *et al.* (2000). The good fit to the SAR data obtained with this very simple approach suggests a possible correspondence between significant features of the slip distribution observed at the surface and the slip distribution on the fault at depth. Regions of relatively higher slip surrounded by regions of lower slip would coincide with well-identified strike-slip segments such as the Karadere, the Sapanca–Akyazi and the Gölçük segments.

The distribution of residuals between the model and the SAR data is represented in Fig. 6(a). Residuals in the far field are flat, of small amplitude and generally negative (except in the NW corner of the scene), indicating that the dislocation model slightly overestimates the overall far-field effect of the earthquake deformation. The broad positive residuals in the NW corner of the scene could correspond to a minor atmospheric effect that we could not remove. Closer to the fault trace the residuals are somewhat larger (up to 6 cm in range) and more conspicuous, both positive and negative. This may imply either local complexities of the actual deformation or local atmospheric effects, which require a more detailed analysis.

A second modelling stage (models IIA and IIB) explores more refined slip distributions over the fault at depth using an inversion procedure and our first-order model as a starting solution. The previous fault is now divided into patches with vertical width of 4 km down to 28 km depth (224 patches, 5×4 km^2). We use a simple iterative linear least-squares inversion procedure (e.g. Ward & Barrientos 1986). Slip is the only free parameter; all other parameters are fixed. For each independent dislocation the problem is linear, but the solution is non-unique and unstable because the solutions on the patches are not independent and the distribution of the data is heterogeneous (Du *et al.* 1992). To evaluate the resolution of the slip on the different regions of the fault we used a truncated singular-value decomposition approach (e.g. Du *et al.* 1992) and smoothed solutions. Introducing artificially small slip perturbations we estimate that smoothed models can resolve a slip of less than 0.5 m in the regions of the fault near the surface ($\leq$12 km depth) and less than 1 m in the regions between 12 and 24 km depth. The models cannot resolve a slip of less than 1 m in regions of the fault at depth greater than 24 km. The resolution of the slip in some regions of the fault at the shallow depth is bad, however, because of the poor coherence of the interferogram in areas close to the fault trace.

Fig. 5 (IIA and IIB) illustrates two different alternatives and Fig. 6 (IIA and IIB) the corresponding residuals. If slip is left free everywhere the solution is very unstable (Fig. 5, IIA). The rms is reduced to 2.1 cm. Slip tends to be more heterogeneously distributed and the regions of higher slip spread towards the sides. Slip in some patches near the surface (0–4 km depth) is inconsistent with the observed surface slip (see Fig. 5b). The most striking inconsistencies are along the Sapanca–Akyazi segment, where modelled slip is much less than observed, and near Izmit, where a patch modelled with very high slip (more than 8 m) seems artificial.

If slip is fixed at the observed values in the patches near the surface and left free elsewhere (Fig. 5, IIB) the solution is more stable. The fit to the data is similar (rms of 2.1 cm) and the regions of higher and lower slip remain well identified. Residuals are generally smaller close to the fault trace (cf. Fig. 6, IIA and IIB) but relatively large positive residuals remain on the northern side of the fault near Izmit. It is probably not coincidence that these residuals are located where high near-surface slip is indicated by the previous inversion (Figs 5, IIA and b). Also the position of these residuals is close to the location of the largest aftershock ($M_l = 6.1$; Özalaybey *et al.* 2002) that occurred on September 13, during the time covered by the SAR images. However, the source of this event is deep (16–18 km; Orgulu & Aktar 2001) and the magnitude moderate, so it is unlikely that it may have modified the fringe pattern significantly.

In a third modelling stage (model III) we seek to reduce residuals close to the fault trace by introducing small changes in the fault dip and rake. After trying different models we retained one with minor down-to-the-north normal movement, consistent with the apparent asymmetry of the fringe gradients in the central part of both the ERS1 and the ERS2 interferograms, as discussed earlier, and with the fault plane solution of the main shock (Fig. 1). Then, we inverted for slip using as an initial solution a slip distribution similar to that obtained in the previous modelling stage (IIB), keeping the near-surface slip fixed. In model III (Fig. 5), all the fault patches of the two central segments (Izmit–Sapanca and Sapanca–Akyazi) have a dip of 85° to the north and a small component of normal faulting (176° rake). The resolution of slip in this model is very similar to that in the vertical model. The rms is now 1.9 cm and the residuals close to Izmit are nearly erased (Fig. 6, III).

The regions with high slip in model III are very similar to those in our first-order model (I) but the progressive fit to the SAR data has caused a cut-off of these regions at different depth. Slip centred in the Sapanca–Akyazi and the Karadere segments appears mostly concentrated in the first 8 km near the surface. In contrast, the region of very high slip centred in Gölçük, immediately west of the hypocentre, seems more deeply rooted (down to 20 km; Fig. 5, III). Total seismic moment and moment magnitude (2.3×10^{20} N m; $M_w = 7.6$) are slightly lower than those in model I, but the fraction of moment released by the Gölçük and nearby segments appears very significant (about two-thirds of the total moment).

Fig. 7 presents the synthetic fringes corresponding to model III, the resulting residual fringes and some selected profiles across the ERS1 data and the model. Overall the synthetic fringes reproduce very accurately the observations (cf. Fig. 7a with Fig. 3a). The excellent fit to the data is also seen in the profiles (Fig. 7c). The maximum amplitude of range change across the fault is about 180 cm (profile 3) corresponding to 4.7 m of horizontal displacement parallel to the fault, which is the value measured in the field at Gölçük and imposed in the inversion. The obtained rms of 1.9 cm corresponds to an error of about 1 per cent. However, it is clear that the very good fit to the SAR data describing the deformation of the Earth's surface corresponds to a much larger uncertainty in the estimates of slip across the fault at depth, due to the increasingly poor resolution of the models. Using the slip data collected in the field at the surface improves the stability of the solutions and reduces the slip uncertainty, as shown.

SECONDARY FAULTING VERSUS ATMOSPHERIC EFFECTS IN GEYVE AND MUDURNU

The main discrepancies between model III and the ERS1 data are in the Geyve and Mudurnu regions. Both the map of residuals and the profiles show short-wavelength residuals of up to 6 cm in range change (Fig. 7b and profiles P1, P2 in Fig. 7c), which coincide with the places where several fringes appear deflected in the two original interferograms (Fig. 3).

These features can be interpreted as slip on secondary faults (e.g. Armijo *et al.* 2000; Wright *et al.* 2001; Feigl *et al.* 2002). After the Izmit earthquake some open cracks were observed along the

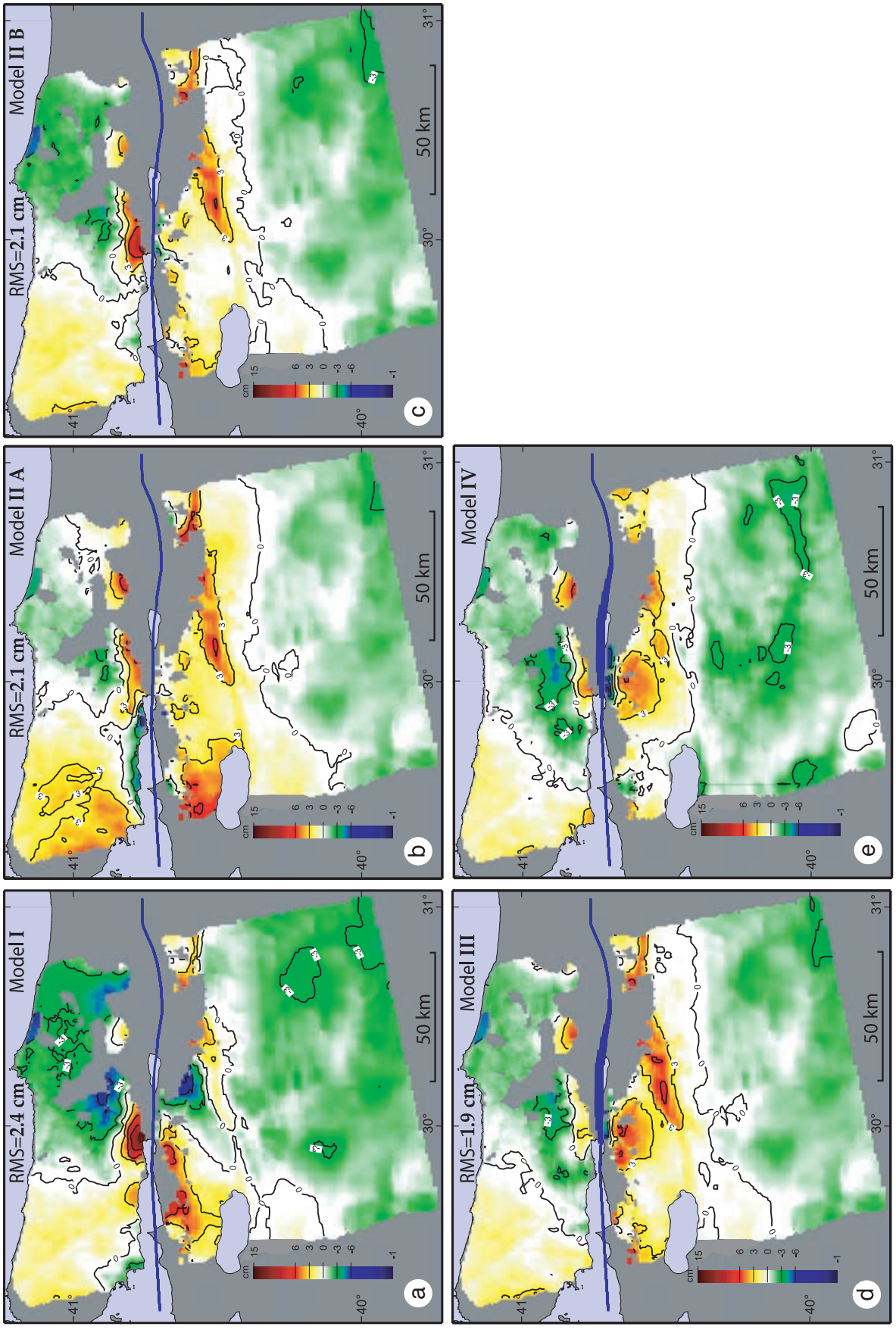

Figure 6. Residual (observed minus modelled) interferograms. The order of the interferograms follows the modelling stages discussed in the text. Residuals are expressed as positive (yellow to red scale) and negative (green to blue scale) values indicating that models, respectively, over or under estimate the surface deformation (the coseismic change in range between the two ERS1 scenes). Residuals are for (a) model I, the first-order forward model (Fig. 5, I); (b) model II, the inversion of slip in all the patches (Fig. 5, IIA); (c) model IIB, the inversion model with slip fixed in the patches near the surface (Fig. 5, IIB); (d) model III, the inversion of slip in a fault allowing for a minor down-to-the-north normal component of slip between Izmit and Akyazi (Fig. 5, III); (e) model IV, the inversion model obtained once a phase delay correlated with the topography is removed from the ERS1 data (see the discussion in the text and Fig. 8c).

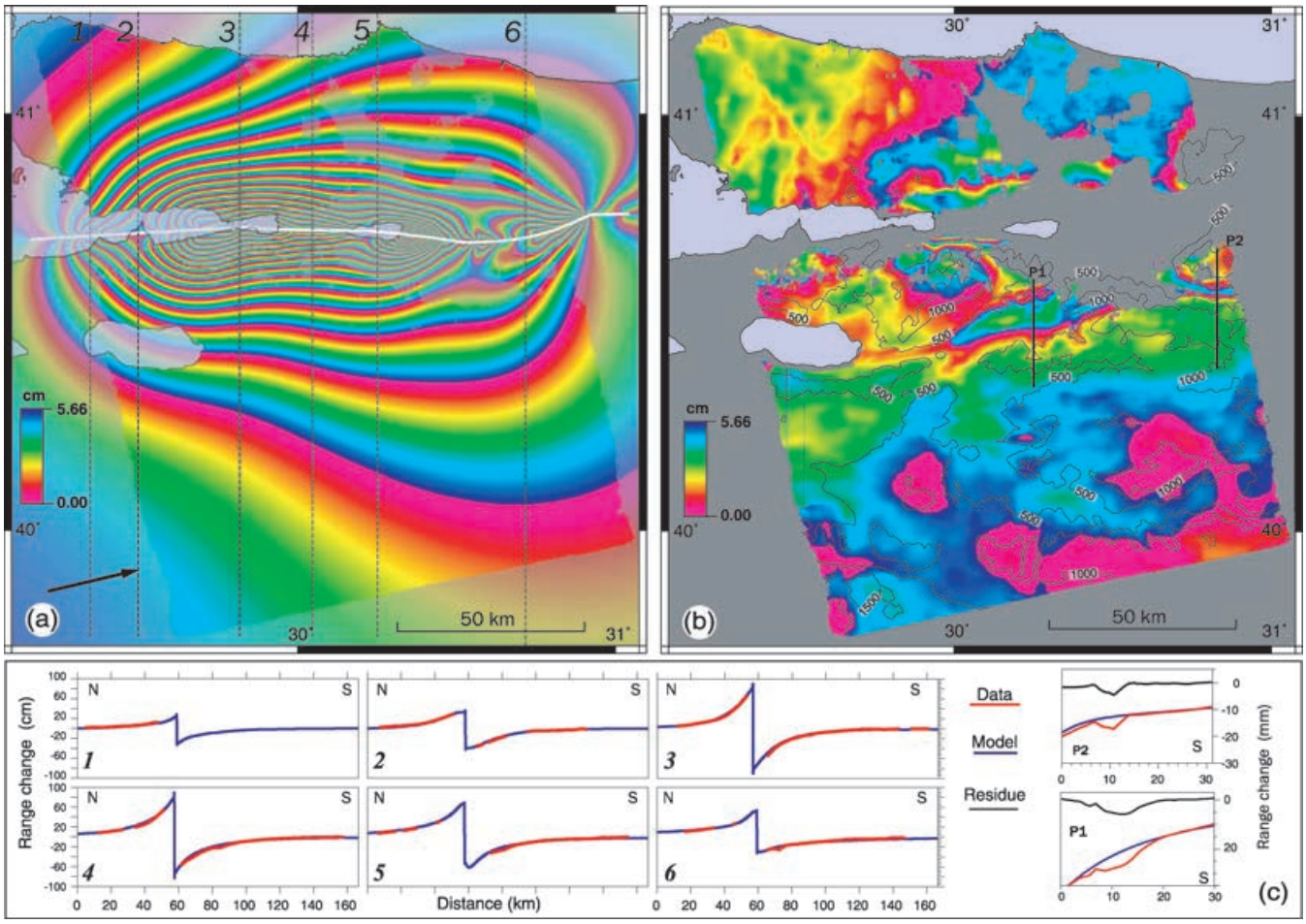

Figure 7. Detailed analysis of model III. (a) Synthetic interferogram. Fringes are emphasized with brighter colours in the coherent parts of the ERS1 interferogram to facilitate comparison with the data shown in Fig. 3(a). The numbered lines indicate the position of the six N–S sections displayed in (c). (b) The residual interferogram is the same as in Fig. 6 (III) but expressed in colour cycles (same colour scale as in a), with elevation contours superimposed every 500 m. The residuals covering the southern region of the interferogram appear closely correlated with the topography. (c) Observed (red) and modelled (blue) profiles of range change across the fault. Significant small-scale misfits are seen across profiles 5 and 6 in the Geyve and Mudurnu regions (boxes labelled P1 and P2, location given in b). These are the two regions where deflected fringes are seen both in the ERS1 and in the ERS2 interferograms (see Fig. 3). The right-hand panel in c gives enlarged profiles of P1, of P2 and of the corresponding residuals (data minus model; black lines).

trace of the Mudurnu Fault, which had ruptured in 1967, but no sign of an earthquake surface break was reported in the Geyve basin area. Wright *et al.* (2001) have modelled these features of the interferograms with a variety of fault kinematics and have preferred models that surprisingly involve left-lateral strike-slip (opposite to the known sense of slip on those faults), which would have been triggered by the main shock. In a similar way Feigl *et al.* (2002) have chosen to model deformation in the Mudurnu valley with right-lateral slip but in the Geyve area with left-lateral slip. Using the known traces of the Mudurnu Fault and that of the fault along the northwestern edge of the Geyve basin (Fig. 2), the two interferometric features can be reproduced reasonably well with right-lateral slip on both faults (Fig. 8a).

Fig. 7(b) shows that the residuals obtained by removing model III from the ERS1 data appear correlated with the topography over a wide area in the southern part of the interferogram. This strongly suggests a change in the tropospheric delay between the acquisition of the two radar scenes (Massonnet & Feigl 1998). The resulting shift in the phase may decrease, linearly or exponentially, with increasing elevation. Overall, the residuals in Fig. 7(b) are well explained with a phase delay that decreases exponentially with elevation (see the caption of Fig. 8c). Adding such a delay to model III provides a satisfactory non-tectonic explanation for the deflected fringes in the Geyve and Mudurnu regions (Fig. 8c). The observation that the short-wavelength noise in the original interferogram (Fig. 8b) appears somewhat reproduced in Fig. 8(c) suggests that this noise is also correlated with the topography.

Thus both secondary faulting and tropospheric effects are able to correctly reproduce the observed features. However, the overall correlation with the topography is robust and there is no indication of the occurrence of large local shocks in Mudurnu and Geyve, simultaneously during the main shock or afterwards. In the ERS2 data of Mudurnu the short-wavelength signal does not appear to correlate perfectly well with the topography, which may suggest some fault slip (Wright *et al.* 2001). We conclude that the most significant part of the deflected fringes in the interferograms must result from a tropospheric effect. The tectonic explanation is possible, but its significance is difficult to assess.

Finally, the tropospheric effect in Fig. 8(c) can be directly removed from the ERS1 data and the resulting interferogram inverted

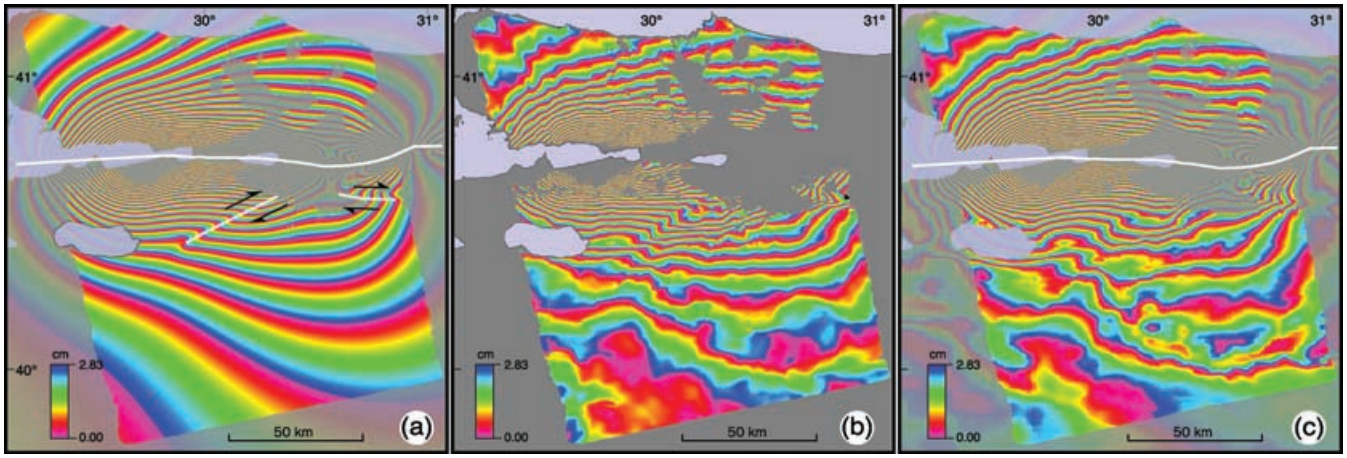

Figure 8. Modelling deflected fringes in the regions of Geyve and Mudurnu. For clarity here each colour cycle represents 2.8 cm of range change along the line of satellite sight (the fringe frequency is twice that in previous figures). The observed fringes in the ERS1 interferogram are illustrated in the middle panel (b) to facilitate comparison with the alternatives on the sides. (a) The synthetic fringes modelled by adding to model III right-lateral motion on two secondary faults. The fault model requires the Mudurnu fault with 60°NNE dip, rupture 10 km long and 20 cm of right-slip between 1–15 km depth ($M_o = 1 \times 10^{18}$ N m; $M_w = 5.8$). The NW Geyve fault is vertical with rupture 27 km long and 22 cm of right-lateral slip between 1–5 km depth (Mo 4×10^{17} N m; $M_w = 5.7$). (c) The synthetic fringes obtained by adding to model III an idealized atmospheric effect correlated with the topography. The used effect is a phase delay (PD in cm) that decreases exponentially with increasing elevation (h in m). It is given by PD $= 5.718\,958 \times [1 - \exp(-0.001\,6120h])$. Interestingly, the short-wavelength 'noise' introduced by the topography is similar to the noise in the data.

for slip, using model III as an initial solution. The resulting slip distribution (not shown) is very similar to that of model III. However, the residuals corresponding to this solution (given in Fig. 6e, model IV) illustrate well the extent to which a tropospheric effect can explain the residuals in the Mudurnu and Geyve regions, which were not specifically addressed in our previous models (compare with I, IIA, IIB and III in Fig. 6).

THE WESTERN END OF THE IZMIT RUPTURE

The SAR data can be used to resolve the western end of the Izmit earthquake rupture. Fig. 9 is an enlargement of the data together with two alternative rupture models for this region. Clearly, models with rupture extending significantly westward beyond the Hersek

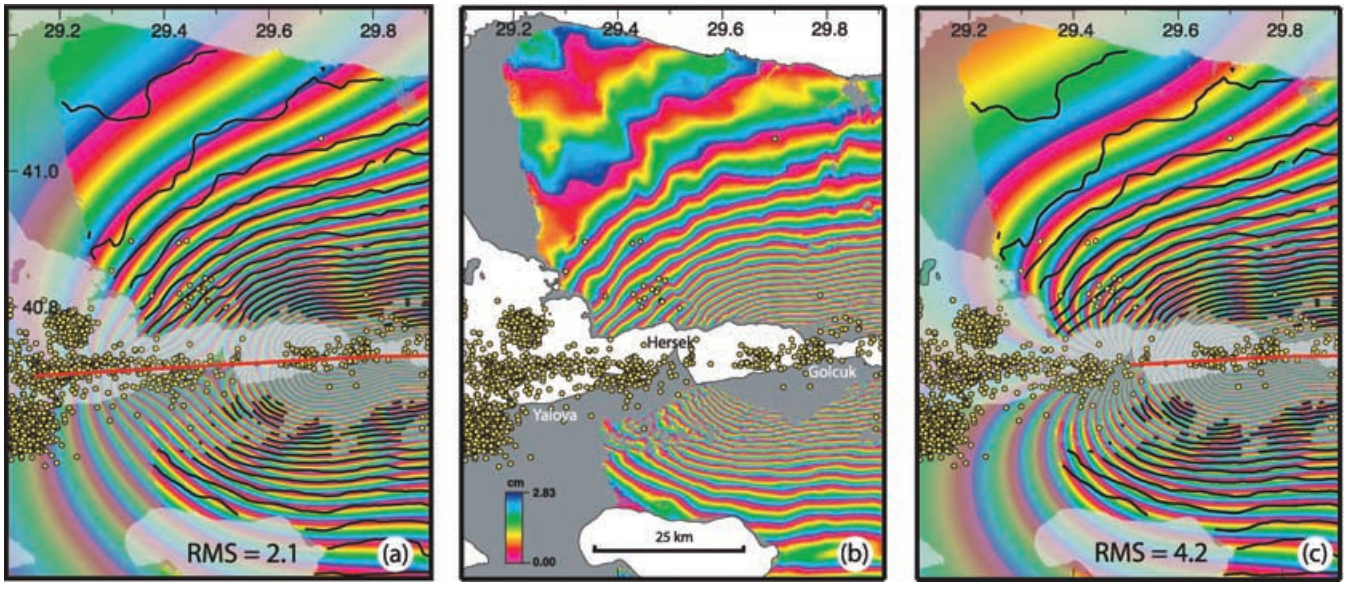

Figure 9. The western end of the Izmit rupture. Yellow circles are aftershocks recorded between 1999 August 20 and October 10 as in Fig. 2. Each fringe represents 2.8 cm of range change, as in Fig. 8. Observed interferogram in the middle panel (b) for comparison with the two alternatives. The rms calculated for this part of the interferogram is given in cm. (a) Synthetic fringes for a rupture extending 30 km west of the Hersek peninsula with the slip distribution of model III (Fig. 5). The simplified Hersek–Yalova fault segment roughly coincides with a cluster of aftershock with almost planar, vertical distribution (Karabulut *et al.* 2002). (c) Synthetic fringes for a rupture ending at the Hersek peninsula. Modelled fault trace in red. Black contour lines overprinted in (a) and (c) were obtained by automatic unwrapping of the observed interferogram. The difference between (a) and (c) is equivalent to $M_o = 1.5 \times 10^{19}$ N m, or an event $M_w = 6.8$, which would have ruptured the Yalova–Hersek segment.

peninsula (Fig. 9a) fit much better the data than models with rupture ending at the Hersek peninsula (Fig. 9b). In model III (Fig. 7a) we have adopted an idealized Yalova–Hersek fault segment geometry consistent with the aftershock distribution and with the position of prominent fault traces in the high-resolution bathymetry (Armijo *et al.* 2002). The modelled fault coincides with an aftershock cluster with an almost planar, vertical distribution of hypocentres (Karabulut *et al.* 2002), which possibly defines the average position of the strike-slip fault segment connecting the Izmit Fault with the more extensional faults bounding the Cinarcik basin. The interferogram does not contain information close to the fault to better constrain complexities of its geometry and kinematics. For instance, there is possibly some normal fault component of slip as the fault enters more and more into the Sea of Marmara. However, the overall symmetry of the observed fringes indicates that no significant normal faulting has occurred and therefore we keep a vertical fault with pure right-slip. Slip across the modelled rupture decreases over 30 km, from 4.5 m in Gölçük to 2 m in Hersek. Then it tapers over the next 30 km (Yalova–Hersek segment), from 2 m to zero (Fig. 5b). Thus a significant average slip of 1–2 m is required down to a depth of 10–15 km across the first 15 km of the latter segment, immediately west of the Hersek peninsula. However, no clear surface break was observed after the Izmit earthquake across the Hersek peninsula (Barka *et al.* 2002). Also, no fresh surface break has yet been detected on the sea bottom during the recent surveys devoted to mapping the submarine part of the fault, west of Hersek (Le Pichon *et al.* 2001; Armijo *et al.* 2002; Polonia *et al.* 2002). Thus the inferred rupture of the Yalova–Hersek segment may have not reached the Earth's surface, although the moment released would have been 1.5×10^{19} N m, equivalent to an event with $M_w = 6.8$.

DIFFERENCES FROM PREVIOUS MODELS: SEPARATING COSEISMIC FROM DEEP-SEATED POST-SEISMIC SLIP

Our preferred slip model (model III, Figs 5, 7, 9a) differs from previous models (Bouchon *et al.* 2000, 2002; Reilinger *et al.* 2000; Yagi & Kikuchi 2000; Feigl *et al.* 2002; Wright *et al.* 2001; Delouis *et al.* 2002). The atmospheric effects in the ERS data, which we have identified, explain some of the discrepancies with other models using the geodetic data (SAR and GPS). However, the most significant improvement comes from the use we make of a precise fault map and of the slip data collected in the field, which reduce the range of possible solutions. However, our model III is consistent with the model proposed by Yagi & Kikuchi (2000), which is derived solely from seismic data (near-field strong motion and teleseismic body wave data).

Another important difference with other approaches concerns the moment release. The moment release in our preferred models (2.3×10^{20} N m) is somewhat higher than that deduced from the seismic records ($1.7–2.0 \times 10^{20}$ N m; Tajima *et al.* 1999; Toksöz *et al.* 1999; Yagi & Kikuchi 2000). The difference may be due to the longer time period (35 days) that is sampled by the SAR interferograms. As stated earlier the SAR interferograms, and thus our models, may contain significant post-seismic deformation. We explore this hypothesis using the published GPS data.

The GPS data include four permanent stations and observations collected in several stations around the fault during many epochs before and soon after the earthquake (Reilinger *et al.* 2000). Reilinger *et al.* (2000) have used this data set to retrieve the horizontal coseismic displacements reproduced in Fig. 10(a), obtained by removing at each non-permanent station the part of the motion attributed to interseismic and to post-seismic deformation. This set of GPS vectors can be used to calibrate a coseismic model derived from our 'longer-period' model III. We adopted the same approach (fixing the same characteristics of the fault and slip near the surface as in model III) to fit the coseismic horizontal displacement at the GPS stations and to obtain the corresponding slip distribution on the fault at depth. The resulting 'purely' coseismic model can be compared with model III (Figs 10c and b, respectively).

Overall the observed horizontal vectors are correctly reproduced by the 'purely' coseismic model (rms = 4 cm), with the exception of a few stations close to the fault, which may be affected by spurious surface effects. Both the predicted coseismic displacement and the GPS vectors in the far field (specifically to the north and south of Izmit, at 10–80 km distance from the fault trace) appear systematically smaller (3–6 cm) than the corresponding horizontal displacement vectors predicted by our 'longer-period' model III (Fig. 10a). Similarly, the modelled coseismic slip on the fault at depth is smaller than the slip in model III (Figs 10c and b) and the coseismic moment of 1.9×10^{20} N m is close to the seismological estimates. The difference in slip between the two models (Fig. 10d) represents the after-slip that may have occurred in the month following the earthquake. There is some 'noise' possibly due to some GPS stations close to the fault and to second-order defects of the models. However, zones with positive slip ($\geq$0.8 m) emerge above the noise. Some of these zones are located at 4–16 km depth under regions of low coseismic slip and they are outlined by aftershock activity. Examples are below the bend area of Akyazi in the central part of the rupture, and below the Karadere segment at the eastern end of the rupture. Altogether these shallow after-slip regions represent a small moment release ($\leq 1 \times 10^{19}$ N m). They may be interpreted to occur in velocity strengthening regions of the fault (Tse & Rice 1986). It is clear, however, that the most significant and well-resolved after-slip is found in the more deeply seated region of the fault below Izmit and Gölçük. The part of the signal corresponding to this zone of large after-slip in the interferogram is a set of paired lobes of fringes enclosing slopes with opposite sign, which are symmetrically arranged on both sides of the fault trace (Fig. 11). It is very improbable that such a complicated feature could have resulted from an atmospheric effect and we favour a tectonic origin. Thus the excess of slip in model III strongly suggests that after-slip reaching 2 m has occurred during the month following the main shock, within a zone of the fault located at 12–24 km depth below the epicentral region. The corresponding moment release (0.3×10^{20} N m) is equivalent to an event with $M_w = 7.0$ and represents about 14 per cent of the total moment in model III. Therefore, the difference in moment release between the 'longer-period' model III and the seismological estimates appears to be explained by the occurrence of aseismic after-slip, deeply seated across the fault zone below the epicentral region.

SLIP HETEROGENEITY, FAULT SEGMENTATION AND SIGNIFICANCE OF THE RAPID AFTER-SLIP

Although broadly corroborating the interpretation of Reilinger *et al.* (2000), our coseismic model, calibrated with the same GPS measurements, is simpler and appears more robust. It is consistent with the well-resolved features of the SAR interferometry and the tectonic observations. The modelling approach also allows us to discuss the geometrical relation between the fault segments, the location

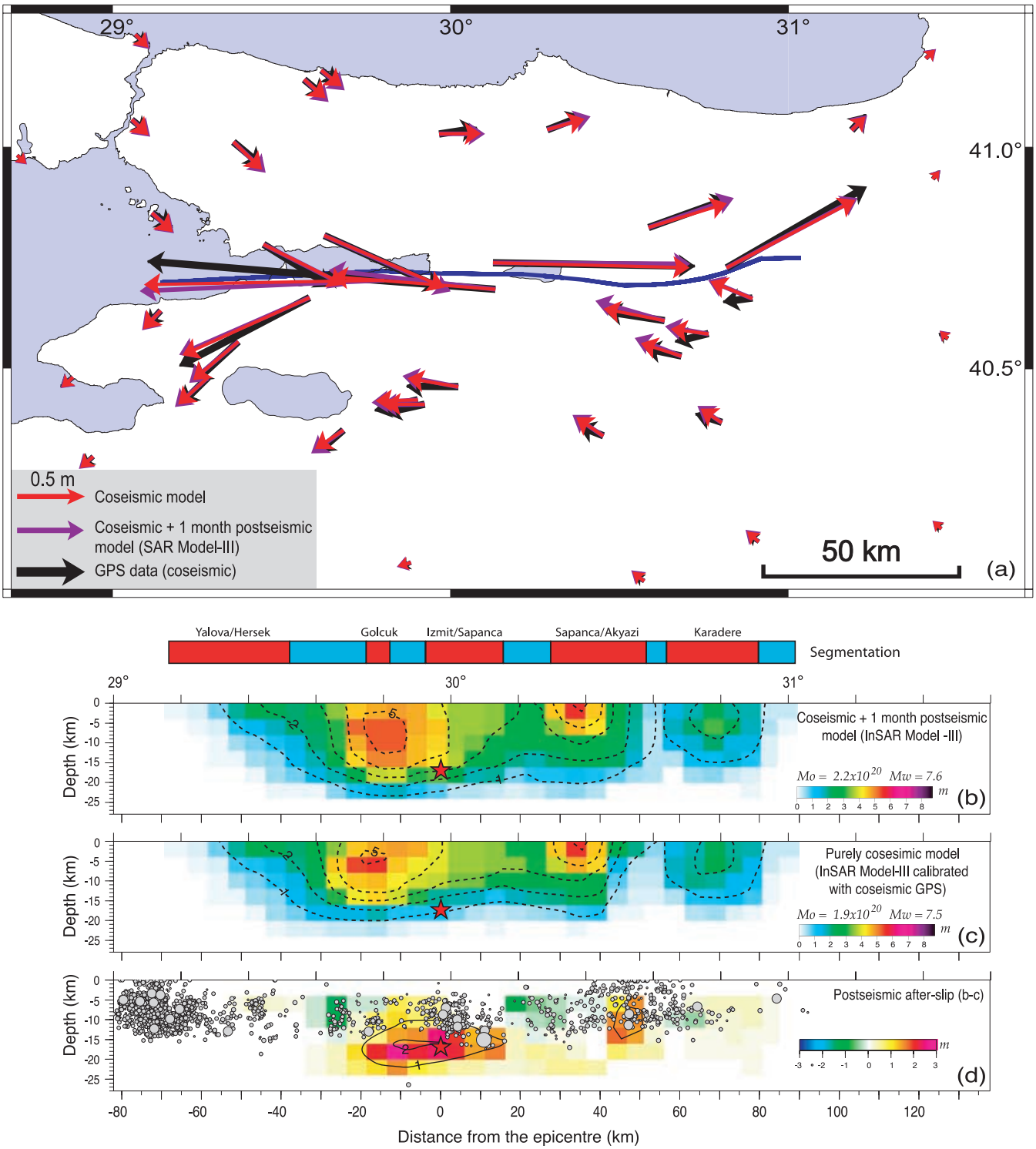

Figure 10. Separating the early after-slip from the 'purely' coseismic slip. (a) Horizontal displacement is represented at the GPS stations. The coseismic GPS observations (black arrows) are from Reilinger *et al.* (2000). The vectors in violet are predicted from the 'longer-period' model III represented in (b), which includes the 29 days of post-seismic deformation captured by the ERS1 data. The vectors in red correspond to the coseismic model represented in (c), which is derived from the same geometry and kinematics as model III, but calibrated to fit the coseismic GPS data. The blue line is the simplified fault trace. The difference between (b) and (c) corresponds to the after-slip shown in (d). The red stars represent the main shock hypocentre. Aftershocks are in grey.

of the hypocentre and the slip distribution, either coseismic or the after-slip, and to draw simple mechanical inferences that differ from earlier inferences in some important aspects (Reilinger *et al.* 2000; Bürgmann *et al.* 2002; Hearn *et al.* 2002).

Both the 'longer-period' model III and the 'purely' coseismic (GPS-derived) model indicate heterogeneous slip with three main zones of higher slip. Two of these zones correspond unequivocally to individual fault segments that are well identified in the surface

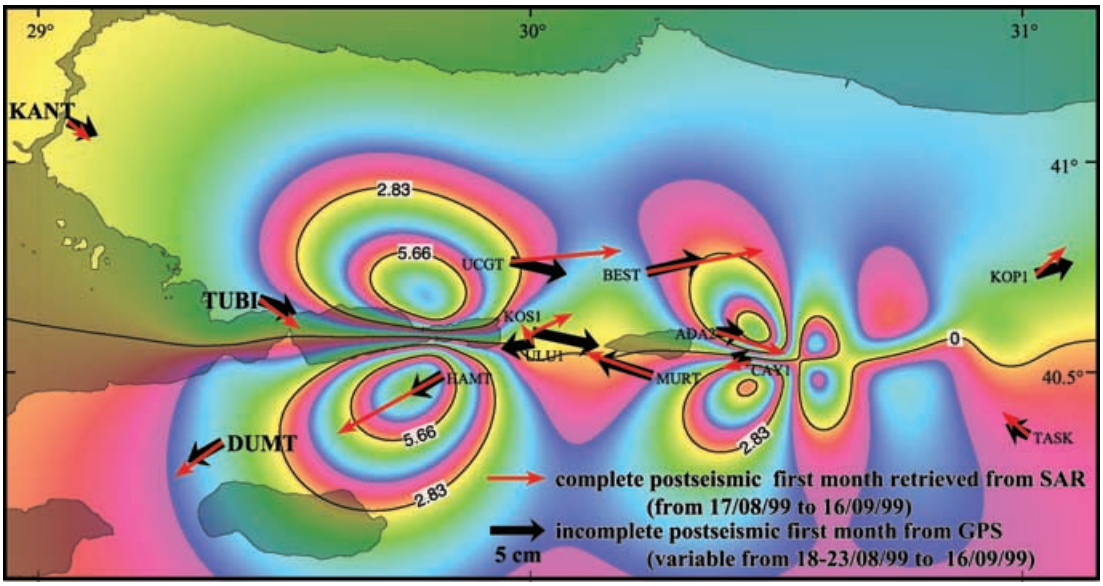

Figure 11. Post-seismic deformation of the Earth's surface. The synthetic fringes represent the range change (in cm) corresponding to our after-slip model, as retrieved from the ERS1 data and depicted in Fig. 10(d). It seems improbable that such a set of fringes including symmetric paired lobes on both sides of the fault could be an atmospheric effect included in the data. The corresponding horizontal displacement (in red) can be compared with the total displacement observed with GPS during the first 29 days after the mainshock (in black). The GPS data set on continuously recording stations shows rapidly decaying deformation but the record is not complete (Bürgmann *et al.* 2002). The three stations in bold (KANT, TUBI and DUMT) are permanent stations already installed before the mainshock. The other stations were installed within few days following the mainshock and they do not include the deformation that may have occurred during the first 2–3 days after the mainshock. The large differences between the red and black arrows may be explained by very rapid, early after-slip reaching 1 m that may have occurred in the region of Gölçük, around and below the hypocentre.

morphology, namely the Sapanca–Akyazi and the Karadere segments. However, the third and largest zone of high slip, centred in the Gölçük segment but also comprising the Yalova–Hersek and the Izmit–Sapanca segments, is different: it extends through significant fault stepovers. This larger zone contributes two-thirds of the total moment in the 'longer-period' model III and it is interesting to note that the hypocentre of the main shock is located at its edge. In terms of slip distribution the Izmit rupture has smoothed out the fault complexities (velocity strengthening regions) within the zone with maximum moment release around Gölçük. This feature is consistent with the idea that under the Gölçük region a large slip deficit and possibly a large elastic loading existed prior to the earthquake. It is also consistent with the occurrence of small events in this region in the years before the main shock (Baris *et al.* 2002). Nucleation of large events at the edges of zones with high coseismic slip have been described elsewhere (Archuleta 1984).

For the three main zones of higher slip the lower cut-off in the coseismic slip occurs at about 15 km depth. However, the after-slip zone appears to extend well into the lower crust, down to 20–25 km depth, directly under the zone of highest moment release and the main shock hypocentre. Thus, the most important after-slip does not appear to be concentrated under segments with relatively little coseismic slip, as suggested by Reilinger *et al.* (2000). Although the resolution in the depth estimate for the after-slip is poor (that of the SAR data modelling, discussed earlier), the inference that significant after-slip has occurred down to at least this depth range suggests static stress changes triggered by the earthquake over the same depth. This depth range also seems to be in keeping with the lateral extent (along strike) of the Gölçük high-slip region. Thus the rapid localized after-slip under Gölçük requires an elastic response of the mid-lower crust and accelerated aseismic shear across the fault zone. The Gölçük after-slip zone encompasses a region of the fault having substantial coseismic slip, including the hypocentre. This alternating behaviour suggests that the after-slip zone is located at the transition between an upper region of the fault dominated by stick–slip (seismogenic) and a lower region dominated by plastic shear (aseismic). Our results suggest that the rapid after-slip has penetrated deeply into the latter.

The SAR data must include all the post-seismic deformation during the first 29 days following the earthquake and our results can be checked for consistency with models derived from the GPS data, which have less complete coverage in space and time. The zone of fast after-slip under Gölçük and Izmit that we deduce from the interferograms has been roughly depicted by Reilinger *et al.* (2000) using the post-seismic GPS data (see their fig. 3c). Yet, more recent analyses of the GPS data suggest that the highest amount of after-slip has occurred below the Karadere Fault segment, at the eastern end of the rupture (Bürgmann *et al.* 2002; Hearn *et al.* 2002). The most important discrepancy with our inferences is that none of the models derived from the GPS data predicts more than 0.4 m of after-slip during the 75–80 days following the main shock. Another difference concerns the depth to which the after-slip has penetrated. Bürgmann *et al.* (2002) and Hearn *et al.* (2002) suggested after-slip of 10–40 cm down to depths of 40 km. We find that a region with slip of 1–3 m at 18 km depth is well resolved in our SAR models, while neither the SAR nor the GPS data can resolve slip of a few tens of centimetres in regions of the fault at more than 24 km depth.

The deformation field associated with the region of high after-slip below Gölçük during the first 29 days after the main shock can be compared directly with the corresponding deformation deduced from the published GPS records. These records show deformation rapidly decaying with time after the main shock (Bürgmann *et al.* 2002). From the 13 permanent GPS stations available for the

region, only three were in operation prior to the main shock and have thus captured without interruption all the post-seismic deformation (KANT, TUBI, DUMT; Fig. 11). The total horizontal displacement in these stations during this critical period of time (17 August to 16 September) is consistent, within uncertainties, with the vectors predicted by the large after-slip below Gölçük (Fig. 11). The remaining 10 GPS stations started to be installed in the near field of the fault in the days following the earthquake. The earliest reliable daily solutions are available only 2 days after the main shock. For these stations the total post-seismic displacement recorded (between the date of each first solution and 16 September) is thus not complete, but it is worth comparing it with the corresponding vectors predicted by our after-slip model (Fig. 11). Most of the vectors in the two sets have compatible directions. However, the vector magnitudes required by the large after-slip below Izmit–Gölçük are larger than the observed GPS vectors. This discrepancy is especially clear for stations around Izmit (HAMT, UCGT, BEST, MURT), where the after-slip requires about twice as much as the GPS vectors. For the station placed near the eastern end of the rupture, however, (KOP1), the two vectors are nearly coincident. We conclude that about half of the large after-slip determined with the SAR data below Izmit–Gölçük may have occurred during the first 2 days following the main shock. The rapidity of this large early after-slip would explain why it has not been incorporated in the models derived from the GPS data alone (Bürgmann *et al.* 2002; Hearn *et al.* 2002). If this line of reasoning is correct, then the maximum after-slip of about 2 m at 16–18 km depth near the hypocentre would have started to occur at rates of up to 180 m yr^{-1} (1 m in 2 days), which is significantly faster (two orders of magnitude) than deduced earlier (Bürgmann *et al.* 2002). Nevertheless, our results are not inconsistent with the main inference from the GPS modelling, indicating that a significant albeit much smaller amount of after-slip has occurred below the Karadere fault segment, at the eastern end of the rupture (Bürgmann *et al.* 2002; Hearn *et al.* 2002).

IMPLICATIONS CONCERNING THE LONG-TERM GEOLOGICAL RECORD

The correlation between the coseismic slip at depth and the measured slip along the surface rupture is good, indicating that slip distribution at the surface is representative of that at depth. In retrospect this observation makes the surface slip distributions measured for earlier earthquakes along the NAF more meaningful (Barka 1996). However, the coseismic slip is unevenly correlated with the long-term fault segmentation seen in the morphology. The coseismic slip distribution reproduces sharply the shape of the Sapanca–Akyazi and the Karadere segments along the eastern part of the rupture, but the boundaries between individual segments are not visible in the slip distribution for this earthquake around the high-slip region around Gölçük. Brecciation mechanisms across fault jogs at segment boundaries may explain such features (e.g. King 1983; Sibson 1986). Then it seems possible to make a distinction between two different modes of rupture: an overloaded segment mode in Gölçük, which is capable of 'erasing' the jogs at segment boundaries, and a critically loaded segment mode, which prevents the segment boundaries from high coseismic slip so that its long-term shape is preserved. Both have been favourable to the propagation of the Izmit rupture over its 160 km length along strike (e.g. Harris *et al.* 2002). However, the rupture stopped at the eastern end of the Karadere segment and the $M_w = 7.2$ Düzce earthquake ruptured the next individual segment, 3 months later, with a slip distribution comparable to that of the Sapanca–Akyazi segment (Akyüz *et al.* 2002). Thus this latter segment also ruptured apparently under a critically loaded mode. This shows that even under sufficient tectonic load, individual segments may or may not rupture in a concatenation of subevents involving their neighbouring segments. Conversely, it seems unlikely that the segment boundaries would have been enough to arrest the Izmit rupture inside the region of inferred large slip deficit and elastic overload, which may have existed in Gölçük prior to the earthquake. In other words, once triggered, the Izmit earthquake could not have been smaller than the size of the overloaded region around Gölçük. There the slip deficit had probably grown larger than the slip that any of the small individual fault segments visible at the surface could undergo alone, without having a high associated stress drop and producing high stress concentrations at the segment edges. The large coseismic slip in the overloaded region around Gölçük has also immediately triggered particularly large and fast after-slip in the velocity-strengthening region of the fault immediately below.

The particular conditions around Gölçük may have also influenced the rupture propagation. The very short *S–P* time (1.78 s) observed in a strong-motion station located beside the Sapanca–Akyazi segment 40 km east of the mainshock hypocentre can be interpreted in two alternative ways: it could be the effect of either a supershear rupture propagation, or the triggering of an asperity by the *P*-wave arrival from the hypocentre (Bouchon *et al.* 2001; Sekiguchi & Iwata 2002). Both our inference of an overloaded region around the epicentral region and the observation of an extensional jog with less coseismic slip at the Sapanca lake give support to the triggered asperity hypothesis, albeit without contradicting the supershear rupture propagation.

The arguments above suggest that a heterogeneous slip and loading distribution along a large fault system such as the North Anatolian Fault may control propagation of large earthquake ruptures. For such a system, the notion of 'characteristic earthquake' (Schwartz & Coppersmith 1984) would apply only to the critically loaded mode of rupture along individual segments. However, it will be very difficult to deduce from the surface slip distribution alone whether contiguous segments with 'characteristic ruptures' have ruptured together or not. In addition, the amount of coseismic slip on any segment will depend on variable degrees of slip deficit and load, or 'excess load'. Overloaded segments possibly undergo more slip than scaling laws would predict. These features are of concern to inferences of rupture length and moment magnitude for past earthquakes deduced from trenching. To describe distinct past events such as the Izmit and the Düzce earthquakes would require relying upon the resolution of many measurements of slip along the fault trace and upon many well-resolved dates (provided that the events are separated by a reasonably long time interval).

Part of the heterogeneity in the loading along the NAF is likely to result from the fault segmentation, which may scale with the thickness of the seismogenic crust and may evolve as an effect of wear during progressive slip and fault growth (e.g. Scholz 1987). However, large stress heterogeneities (as in Gölçük) may also have grown up and evolved from an uneven slip distribution during previous events. Thus the critical datum appears to be the distribution of slip deficit along the fault. For any segment along the NAF and at any time the state of loading must integrate a complex slip history including sequences of earthquakes that probably never repeat in the same way. The observations presented here give support to a variable slip model incorporating large earthquakes with variable magnitude and rupture length, which would result from unsteady segment-to-segment rupture propagation (from overloaded segments to critically loaded segments and vice versa).

SUMMARY

Combining the SAR interferometry with the tectonic observations appears to be a powerful approach to resolving the features of the slip distribution associated with the 1999 August 17 Izmit earthquake. In this work the fault geometry, the fault kinematics and the near-field deformation are resolved using well-constrained tectonic observations collected in the field.

The SAR data set provides the best overall image of the surface deformation and appears to be the most appropriate set for deducing an overall image of the static rupture at seismogenic depth. However, the possible occurrence of atmospheric effects may hinder a good solution. A critical analysis of the SAR data using a pairwise logic approach and independent meteorological data (from NOAA satellite images) allow us to identify atmospheric effects and to remove them from subsequent modelling.

To calculate the slip distribution we use dislocations in elastic half-space and an overall forward modelling strategy, which combines a trial-and-error approach with a conventional inversion technique. Improving the data fits by steps seems more appropriate than uncontrolled inversion.

Slip is underdetermined, but the use of well-constrained measurements of slip at the Earth's surface reduces the range of possible solutions considerably. The uncertainty in our slip estimates increases with depth. A good fit to the SAR data (rms of less than 2 cm) corresponds to a slip resolution of less than 0.5 m in the regions of the fault near the surface ($\leq$12 km depth) and less than 1 m in the regions between 12 and 24 km depth. However, the models cannot resolve a slip of less than 1 m in regions of the fault at depth greater than 24 km.

The best fits to the SAR data define an inhomogeneous slip distribution with three main zones of high slip along the fault and a total moment release of 2.3×10^{20} ($M_w = 7.6$). The inhomogeneous slip distribution correlates well with the overall geometry of the fault segmentation, which is well defined from the morphology.

The Izmit earthquake rupture appears to have extended well into the eastern Sea of Marmara. The SAR data indicate that the Yalova–Hersek segment ruptured for 30 km west of the Hersek peninsula, with slip tapering westwards from 2 m to zero and a moment release of 1.5×10^{19} N m, equivalent to an event $M_w = 6.8$. The western end of the rupture is located 40 km SSE from downtown Istanbul.

The SAR data show two sets of deflected fringes in the valleys of Mudurnu and Gevye, which have been previously interpreted as resulting from slip triggered on secondary faults. We show that these features mostly result from atmospheric effects correlated with the topography. A tectonic explanation is possible, but its significance is difficult to assess.

The ERS1 SAR interferogram, and thus our models, cover a 'long period' as they include the 29 days following the main shock and they may contain significant post-seismic deformation. Using our 'longer-period model' and the published GPS data describing the coseismic horizontal deformation (Reilinger *et al.* 2000) we have derived a slip model that better represents the coseismic slip alone. This model suggests that the moment release corresponding to the main shock is 1.9×10^{20} N m ($M_w = 7.5$), which is close to the seismological estimates.

The foregoing approach allows us to retrieve the early post-seismic deformation that has been captured by the SAR data. The difference in moment release between our 'longer-period' model and the seismological estimates appears to be explained by the occurrence of fast aseismic after-slip, reaching 2 m during the month following the main shock, within a zone of the fault located at 12–24 km depth, directly under the zone of highest moment release in Gölçük. The Gölçük after-slip zone encompasses a region of the fault having substantially slipped coseismically, including the hypocentre.

Comparison of the after-slip retrieved from the SAR with the available GPS records of post-seismic deformation (Bürgmann *et al.* 2002) suggests that about half of the after-slip captured by the SAR data below Izmit–Gölçük may have occurred during the first 2 days following the main shock. The rapidity of the early after-slip would explain why it has not been incorporated in the models derived from the GPS data alone (Bürgmann *et al.* 2002; Hearn *et al.* 2002). Accordingly, the maximum after-slip of 2 m at 16–18 km depth near the hypocentre would have started immediately after the mainshock at very fast rates (up to 1 m in 2 days).

The correlation between the coseismic slip on the fault at depth and slip measured along the surface break is good, indicating that slip distribution at the surface is representative of that at depth. However, slip is unevenly correlated with the long-term fault segmentation: the Izmit earthquake slip distribution reproduces well the shape of some segments with a 'characteristic rupture' (Sapanca–Akyazi and Karadere segments), but it has smoothed out the fault complexities at the boundaries between individual segments around the high-slip region of Izmit–Gölçük. This suggests that under the Gölçük region a large slip deficit and possibly a large elastic loading existed prior to the earthquake. This feature is consistent with the occurrence of both the rapid early after-slip under the overloaded region and the small events in this region in the years preceding the main shock.

The heterogeneous coseismic slip and the state of loading on the different segments of the NAF may result from a heterogeneous distribution of slip deficit accumulated during previous large earthquakes. In turn, the slip history and associated stress heterogeneities may be important factors controlling the occurrence of moderate and large earthquakes with variable magnitude and rupture length, resulting from unsteady segment-to-segment rupture propagation along the North Anatolian Fault.

ACKNOWLEDGMENTS

This work is part of Ziyadin Çakir's PhD thesis with Aykut Barka and Rolando Armijo as co-advisors, under an agreement between our two institutions (ITU and IPGP). It has been performed within the framework of the collaborative programme on the seismic risk in the Istanbul and Sea of Marmara region coordinated by the Turkish TUBITAK and the French INSU-CNRS, with support from the French Ministry of Foreign Affairs (MAE). For the access to the ERS imagery, critical to this study, we benefited from constant help and advice from the European Space Agency (ESA) under contract AO3-354. We thank Geoffrey King, Peter Molnar and especially Renata Dmowska for their sympathetic criticism, which helped to improve the manuscript. Tim Wright and Roland Bürgmann gave helpful reviews. This is Institut de Physique du Globe de Paris (IPGP) paper no 1914.

REFERENCES

Akyüz, H.S., Hartleb, R., Barka, A., Altunel, E., Sunal, G., Meyer, B. & Armijo, R., 2002. Surface rupture and slip distribution of the 12 November 1999 Düzce earthquake (*M* 7.1), north Anatolian Fault, Bolu, Turkey, *Bull. seism. Soc. Am.,* **92,** 61–66.

Archuleta, R.J., 1984. A faulting model for the 1979 Imperial Valley earthquake, *J. geophys. Res.,* **89,** 4559–4585.

Armijo, R., Meyer, B., Hubert, A. & Barka, A., 1999. Westward propagation of the North Anatolian Fault into the northern Aegean: timing and kinematics, *Geology,* **27,** 267–270.

Armijo, R., Meyer, B., Barka, A., de Chabalier, J.B. & Hubert, A., 2000. The fault breaks of the 1999 earthquakes in Turkey and the tectonic evolution of the Sea of Marmara: a summary, 55–62, in *The 1999 Izmit and Düzce Earthquakes: Preliminary Results,* eds Barka, A., Kozaci, O., Akyüz S. & Altunel E., Istanbul Technical University, Istanbul.

Armijo, R., Meyer, B., Navarro, S., King, G. & Barka, A., 2002. Asymmetric slip partitioning in the Sea of Marmara pull-apart: a clue to propagation processes of the North Anatolian Fault?, *TerraNova,* **14,** 80–86.

Atakan, K., Ojeda, A., Meghraoui, M., Barka, A., Erdik, M. & Bodare, A., 2002. Seismic hazard in Istanbul following the 17 August and 12 November 1999 Düzce earthquakes, *Bull. seism. Soc. Am.,* **92,** 466–482.

Baris, S., Ito, A., Ücer, S.B., Honkura, Y., Kafadar, N., Pektas, R., Komut, T. & Iskara, A.M., 2002. Microearthquake activity before the Izmit earthquake in the eastern Marmara region, Turkey (1 January 1993–17 August 1999), *Bull. seism. Soc. Am.,* **92,** 394–405.

Barka, A., 1996. Slip distribution along the North Anatolian Fault associated with the large earthquakes of the period 1939–1967, *Bull. seism. Soc. Am.,* **86,** 1238–1254.

Barka, A., 1999. The 17 August 1999 Izmit earthquake, *Science,* **285,** 1858–1859.

Barka, A. & Kadinsky-Cade, K., 1988. Strike-slip fault geometry in Turkey and its influence on earthquake activity, *Tectonics,* **7,** 663–684.

Barka, A. *et al.,* 2002. The surface rupture and slip distribution of the 17 August 1999 Izmit earthquake *M* 7.4, North Anatolian fault, *Bull. seism. Soc. Am.,* **92,** 43–60.

Beauducel, F., Briole, P. & Froger, J.L., 2000. Volcano wide fringes in ERS synthetic aperture radar interferograms of Etna: deformation or tropospheric effect, *J. geophys. Res.,* **105,** 16 391–16 402.

Bouchon, M., Toksöz, N., Karabulut, H., Bouin, M.-P., Dietrich, M., Aktar, M. & Edie, M., 2000. Seismic imaging of the Izmit rupture inferred from the near-fault recordings, *Geophys. Res. Lett.,* **27,** 3013–3016.

Bouchon, M., Bouin, M.-P., Karabulut, H., Toksöz, M.N., Dietrich, M. & Rosakis, A.J., 2001. How fast is rupture during an earthquake? New insights from the 1999 Turkey earthquakes, *Geophys. Res. Lett.,* **28,** 2723–2726.

Bouchon, M., Töksoz, M.N., Karabulut, H., Bouin, M.P., Dietrich, M., Aktar, M. & Edie, M., 2002. Space and time evolution of rupture and faulting during the 1999 the Izmit (Turkey) earthquake, *Bull. seism. Soc. Am.,* **92,** 256–266.

Bürgmann, R., Ergintav, S., Segall, P., Hearn, E.H., McClusky, S., Reilinger, R.E., Woith, H. & Zschau, J., 2002. Time-dependent distributed afterslip on and deep below the Izmit earthquake rupture, *Bull. seism. Soc. Am.,* **92,** 126–137.

Delacourt, C., Briole, P. & Achache, J., 1998. Tropospheric corrections of SAR interferograms with strong topography: application to Etna, *Geophys. Res. Lett*., **25,** 2849–2852.

Delouis, B., Giardini, D., Lundgren, P. & Salichon J., 2002. Joint inversion of InSAR, telesesimic and strong motion data for the spatial and temporal distribution of earthquake slip: application to 1999 Izmit main shock, *Bull. seism. Soc. Am.,* **92,** 278–299.

Du, Y., Aydin, A. & Segall, P., 1992. Comparison of various inversion techniques as applied to determination of a geophysical deformation model for the Borah Peak earthquake, *Bull. seism. Soc. Am.,* **82,** 1840–1866.

Ergintav, S., Bürgmann, R., McClusky, Çakmak, R., Reilinger, R.E., Lenk, O., Barka, A. & Özener, H., 2002. Postseismic deformation near the Izmit earthquake (17 August 1999, *M* 7.5) rupture zone, *Bull, seism. Soc. Am.,* **92,** 194–207.

Feigl, K.L. *et al.,* 2002. Estimating slip distribution for the Izmit mainshock from coseismic GPS, ERS-1, RADARSAT, and SPOT measurements, *Bull. seism. Soc. Am.,* **92,** 138–160.

Gabriel, A.K., Goldstein, R.M. & Zebker, H.A., 1989. Mapping small elevation changes over large areas: differential radar interferometry, *J. geophys. Res.,* **94,** 9183–9191.

Goldstein, R.M. & Werner, C.L., 1998. Radar interferogram filtering for geophysical applications, *Geophys. Res. Lett.,* **25,** 4035–4038.

Harris, R.A., Dolan, J.F., Hartleb, R. & Day, S.M., 2002. The 1999 Izmit, Turkey, earthquake: a 3-D dynamic stress transfer model of intraearthquake triggering, *Bull. seism. Soc. Am.,* **92,** 245–255.

Hartleb, R.D. *et al.,* 2002. Surface rupture and slip distribution along the Karadere segment of the 17 August 1999 Izmit and the western section of the 12 November 1999 Düzce, Turkey, earthquakes, *Bull. seism. Soc. Am.,* **92,** 67–78.

Hearn, E.H., Bürgmann, R. & Reilinger, R.E., 2002. Dynamics of Izmit earthquake postseismic deformation and loading of the Düzce earthquake hypocenter, *Bull. seism. Soc. Am.,* **92,** 172–193.

Hubert-Ferrari, A., Barka, A., Jacques, E., Nalbant, S.S., Meyer, B., Armijo, R., Tapponnier, P. & King, G.C.P., 2000. Seismic hazard in the Marmara Sea following the 17 August 1999 Izmit earthquake, *Nature,* **404,** 269–273.

Ito, A. *et al.,* 2002. Aftershock activity of the 1999 Izmit, Turkey, earthquake, revealed from microearthquake observations, *Bull. seism. Soc. Am.,* **92,** 418–427.

Karabulut, H., Bouin, M.P., Bouchon, M., Dietrich, M., Cornou, C. & Aktar, M., 2002. The seismicity in the eastern Marmara Sea after the 17 August 1999 Izmit earthquake, *Bull. seism. Soc. Am.,* **92,** 387–393.

King, G.C.P., 1983. The accommodation of strain in the upper lithosphere of the Earth by self-similar fault systems; the geometrical origin of *b*-value, *Pure appl. Geophys.,* **121,** 761–815.

Kuscu, I., Okamura, M., Matsuoka, H. & Awata, Y., 2002. Active faults in the Gulf of Izmit on the north Anatolian Fault, NW Turkey: a high-resolution shallow seismic study, *Mar. Geol.,* **190,** 421–443.

Langridge, R.M., Stenner, H.D, Fumal, T.E., Christoffereson, S.A., Rockwell, T.K., Hartleb, R.D., Bachhuber, J. & Barka, A.A., 2002. Geometry, slip distribution, and kinematics of surface rupture on the Sakarya fault segment during the 17 August 1999 Izmit, Turkey, earthquake, *Bull. seism. Soc. Am.,* **92,** 107–125.

Le Pichon, X. *et al.,* 2001. The active main Marmara fault, *Earth planet. Sci. Lett.,* **192,** 595–616.

Massonnet, D. & Feigl, K.L., 1998. Radar interferometry and its applications to changes in the Earth's surface, *Rev. Geophys.,* **36,** 441–500.

Massonnet, D., Rossi, M., Carmona, C., Adragna, F., Peltzer, G., Feigl, K. & Rabaute, T., 1993. The displacement field of the Landers earthquake mapped by radar interferometry, *Nature,* **364,** 138–142.

Michel, R. & Avouac, J.P., 2002. Deformation due to the 17 August 1999 Izmit, Turkey, earthquake measured from SPOT images, *J. geophys. Res.,* **107,** 10.1029/2000JB000390.

Michel, R., Avouac, J.P. & Taboury J., 1999. Measuring ground displacements from SAR amplitude images: application to the Landers earthquake, *Geophys. Res. Lett.,* **26,** 875–878.

Nalbant, S.S., Hubert A. & King G.C.P., 1998. Stress coupling between earthquakes in northwest Turkey and the North Aegean sea, *J. geopys. Res*., **103,** 14 469–24 486.

Okada, Y., 1985. Surface deformation due to shear and tensile faults in a half-space, *Bull. seism. Soc. Am.,* **75,** 1135–1154.

Orgulu, G. & Aktar, M., 2001. Regional moment tensor inversion for strong aftershocks of the August 17, Izmit earthquake ($M_w = 7.4$), *Geophys. Res. Lett.,* **28,** 371–374.

Özalaybey, S., Ergin, M., Aktar, M., Tapırdamaz, C., Biçmen, F. & Yörük, A., 2002. The 1999 Izmit earthquake sequence in Turkey: seismological and tectonic aspects, *Bull. seism. Soc. Am.,* **92,** 376–386.

Parke, J. *et al.,* 1999. Active faults in the Sea of Marmara, western Turkey, imaged by seismic reflection profiles, *TerraNova,* **11,** 223–227.

Parsons, T., Shinji, T., Stein, R.S., Barka, A. & Dieterich, J.A., 2000. Heightened odds of large earthquakes near Istanbul: an interaction-based probability calculation, *Science,* **228,** 661–665.

Polonia, A. *et al.,* 2002. Exploring submarine earthquake geology in the Marmara Sea, *EOS, Trans. Am. geophys. Un.,* **83,** 235–236.

Peltzer, G., Crampé, F. & King, G., 1999. Evidence of non linear elasticity of the crust from the M_w 7.6 Manyi (Tibet) earthquake, *Science,* **286,** 272–276.

Reilinger, R.E. *et al.,* 2000. Coseismic and postseismic fault slip for the 17 August 1999 $M = 7.5$, Izmit, Turkey earthquake, *Science,* **289,** 1519–1524.

Rockwell, T.K., Lindval, S., Dawson, T., Langridge, R., Lettis, W. & Klinger, Y., 2002. Lateral offsets on surveyed cultural features resulting from the 1999 Izmit and Düzce earthquakes, Turkey, *Bull. seism. Soc. Am.,* **92,** 79–94.

Scharroo, R. & Visser, P.N.A.M., 1998. Precise orbit determination and gravity field improvement for the ERS satellites, *J. geophys. Res.,* **103,** 8113–8127.

Scholz, C.H., 1987. Wear and gouge formation in brittle faulting, *Geology,* **15,** 493–495.

Schwartz, D.P. & Coppersmith, K.J., 1984. Fault behavior and characteristic earthquakes: examples from the Wasatch and San Andreas Faults, *J. geophys. Res.,* **89,** 5681–5698.

Sekiguchi, H. & Iwata, T., 2002. Rupture process of the 1999 Kocaeli, Turkey, earthquake estimated from strong-motion waveforms, *Bull. seism. Soc. Am.,* **92,** 300–311.

Sibson, R.H., 1986. Brecciation processes in fault zones: Inferences from earthquake rupturing, *Pure appl. Geophys.,* **124,** 159–176.

Stein, R.S., Barka, A. & Dieterich, J.H., 1997. Progressive failure on the North Anatolian fault since 1939 by earthquake stress triggering, *Geophys. J. Int.,* **128,** 594–604.

Tajima, F., Dreger, D., Breger, L., Uhrhammer, R. & Romanowicz, B., 1999. Source rupture of the Aug. 17, 1999 Turkey earthquake and near-source structural effects, *EOS, Trans. Am. geophys. Un.*, supp., **80,** 669.

Tibi, R. *et al.,* 2001. Rupture precesses of the 1999 August 17 Izmit and November 12 Düzce (Turkey) earthquakes, *Geopys. J. Int.,* **144,** F1–F7.

Toksöz, M.N., Reilinger, R.E., Doll, C.G., Barka, A.A. & Yalcin, N., 1999. Izmit (Turkey) earthquake of the 17 August 1999: first report, *Seism. Res. Lett.,* **70,** 669–679.

Tse, S. & Rice, J., 1986. Crustal earthquake instability in relation to the depth variation of frictional slip properties, *J. geophys. Res.,* **91,** 9452–9472.

Ward, S.T. & Barrientos, S.E., 1986. An inversion for slip distribution and fault shape from geodetic observations of the 1983, Borah Peak, Idaho, earthquake, *J. geophys. Res.,* **91,** 4909–4919.

Wright, T., Fielding, E. & Parsons, B., 2001. Triggered slip: observations of the 17 August 1999 Izmit (Turkey) earthquake using radar interferometry, *Geophys. Res. Lett.,* **28,** 1079–1082.

Yagi, Y. & Kikuchi, M., 2000. Source rupture process of the Kocaeli, Turkey earthquake of August 17, 1999 obtained by joint inversion of near-field data and teleseismic data, *Geophys. Res. Lett.,* **27,** 1969–1972.